Passive Pitch Control in Marine Hydrokinetic Turbine Blades

Ramona Brockman Barber

A thesis submitted in partial fulfillment of
the requirements for the degree of

Master of Science in Engineering

University of Washington

2014

Reading Committee:

Michael Motley, Chair

Laura Lowes

Brian Polagye

Program Authorized to Offer Degree:
Department of Civil and Environmental Engineering

University of Washington

Abstract

Passive Pitch Control in Marine Hydrokinetic Turbine Blades

Ramona Brockman Barber

Chair of the Supervisory Committee:
Assistant Professor Michael Motley
Department of Civil and Environmental Engineering

Green and renewable energy technologies are becoming more and more necessary as demand for energy grows exponentially around the world. Recently, there has been increased interest in using marine hydrokinetic turbines to generate energy from ocean currents and tidal flows. The blades of these turbines are slender and are subjected to large, dynamic fluid forces; for that reason they are typically constructed from fiber-reinforced composites. The bend-twist deformation coupling behavior of these materials can be hydroelastically tailored such that the pitch angle of the blades will passively change to adapt to the surrounding flow, creating an instantaneous reaction that can improve system performance over the expected life of the turbine. Potential benefits of this passive control mechanism include increased lifetime power generation, reduced hydrodynamic instabilities, and improved load shedding and structural performance.

There are practical concerns, however, that increase the complexity of the design of these bend-twist coupled blades. Large inflow variations in viable locations for turbine implementation combined with system component limitations such as restrictions on the generator and maximum rotational speed require consideration of practical and site-specific constraints. Using a previously validated boundary element method-finite element method solver, this work presents a numerical investigation into the capabilities of passive pitch adaptation under both instantaneous and long-term variable amplitude loading to better describe potential benefits while considering practical design and operational restrictions.

TABLE OF CONTENTS

Page

List of Figures iii

List of Tables vi

Chapter 1: Introduction 1
1.1 Motivation 1
1.2 Previous Work 3
1.2.1 Aerodynamics 3
1.2.2 Hydrodynamics 4
1.3 Research Objectives 9

Chapter 2: Methodology 10
2.1 Fluid-Structure Interaction Modeling 10
2.1.1 Boundary Element Method 10
2.1.2 Finite Element Method 12
2.2 Turbine Design Considerations 14
2.2.1 Control Mechanisms 14
2.2.2 Operational Profile 20
2.2.3 Blade Model 23

Chapter 3: Turbine Performance 26
3.1 Operating Regions 26
3.2 Analysis Method 28
3.3 Performance Evaluation 32

Chapter 4: Structural Response 40
4.1 Blade Loads and Stresses 40
4.2 Predicting Composite Failure 44

Chapter 5: Lifetime Performance 56
5.1 Advanced Blade Model 56
5.2 Long Term Structural Response 60

Chapter 6: Conclusions and Future Work 71
6.1 Conclusions 71
6.2 Future Work 73

LIST OF FIGURES

Figure Number Page

2.1 Relative angles $\alpha(r)$, $\phi(r)$, and $\beta(r)$. 15

2.2 Predicted performance of an adaptive turbine in open water flow considering changing tip speed ratio as a function of V or ω only. 19

2.3 Top: measured flow direction and depth-averaged velocity magnitude data from Admiralty Inlet, WA; Bottom: measured velocity magnitude over depth from Admiralty Inlet, WA. 21

2.4 Average annual distribution of depth-averaged inflow velocities measured at Admiralty Inlet, WA (associated with data shown in Figure 2.3). 22

2.5 Schematic of an axial-flow turbine with a spatially varying effective inflow approximated with a 1/7th-power law. 23

2.6 DOE Reference Model 1 [12]. 25

3.1 General plot of turbine power generated as a function of flow velocity. 27

3.2 Probabilistic plot of power generated per year as a function of inflow velocity. 29

3.3 Coefficients of power and thrust for the 0° reference blade. 30

3.4 Predicted performance of the 0° reference blade. 31

3.5 Predicted performance of the 0° reference blade with adjustments made to account for rated power of the turbine system. 32

3.6 Necessary active pitch adjustment for the 0° reference blade. 33

3.7 Coefficients of thrust and power with and without active pitch adjustment. . 34

3.8 Predicted change in tip pitch angle for the reference (0°) and passively controlled turbine blades. 35

3.9 TSR and active pitch control for the reference (0°) and passively controlled turbine blades. 36

3.10 Predicted power generation of the reference (0°) and passively controlled turbine blades. 37

3.11 Predicted total thrust on the reference (0°) and passively controlled turbine blades. 38

4.1 Highest and lowest maximum blade loads experienced in one rotation by the reference (0°) and passively controlled turbine blades. 41

4.2 Highest and lowest maximum blade stresses experienced in one rotation by the reference (0°) and passively controlled turbine blades. 42
4.3 Turbine blade reference rotational angles. 43
4.4 Blade bending stress (σ_1) on the pressure face (left) and suction face (right) at various blade angles corresponding to $V = 1.7$ for the +15° pitch to feather blade. 45
4.5 Blade bending stress (σ_1) on the pressure face (left) and suction face (right) at various blade angles corresponding to $V = 1.7$ for the −15° pitch to stall blade. 46
4.6 Blade bending stress (σ_1) on the pressure face for the pitch to feather (+15°), pitch to stall (−15°), and reference blades corresponding to $V = 1.7$ at blade angles of 90° (maximum load) and 270° (minimum load). 47
4.7 Examples of various composite failure mechanisms. 49
4.8 Fiber maximum stress failure indices in tension (top) and compression (bottom) for the +15° pitch to feather blade (left) and −15° pitch to stall blade (right). 52
4.9 Hashin matrix failure indices in tension (top) and compression (bottom) for the +15° pitch to feather blade (left) and −15° pitch to stall blade (right). . 53
4.10 Fiber-matrix maximum shear stress failure indices for the +15° pitch to feather blade (left) and −15° pitch to stall blade (right). 54

5.1 Material layers in the balsa core blades. 57
5.2 Change in pitch for the solid and balsa core blade models. 58
5.3 Predicted power generation for the solid and balsa core blade models. 59
5.4 Predicted total thrust on the solid and balsa core blade models. 60
5.5 Fiber maximum stress failure indices in tension (top) and compression (bottom) for the +15° pitch to feather, blasa core blade (left) and −15° pitch to stall, balsa core blade blade (right). 61
5.6 Hashin matrix failure indices in tension (top) and compression (bottom) for the +15° pitch to feather, blasa core blade blade (left) and −15° pitch to stall, balsa core blade blade (right). 62
5.7 Fiber-matrix maximum shear stress failure indices for the +15° pitch to feather, blasa core blade blade (left) and −15° pitch to stall blade, balsa core blade (right). 63
5.8 Change in pitch for the balsa core blade models under degraded strength and stiffness conditions. 65
5.9 Fiber maximum stress failure indices in tension (top) and compression (bottom) for the +15° pitch to feather blade (left) and −15° pitch to stall blade (right) under degraded strength and stiffness conditions. 67

5.10 Hashin matrix failure indices in tension (top) and compression (bottom) for the $+15^\circ$ pitch to feather blade (left) and -15° pitch to stall blade (right) under degraded strength and stiffness conditions. 68
5.11 Fiber-matrix maximum shear stress failure indices for the $+15^\circ$ pitch to feather blade (left) and -15° pitch to stall blade (right) under degraded strength and stiffness conditions. 69

LIST OF TABLES

Table Number Page

2.1 Material Properties of Hexcel IM7-8552 [16]. 24

3.1 Rated speed and maximum pitch change of the various turbine blades considered. 39

4.1 Methods of predicting composite failure mechanisms used in this work. 51

5.1 Material Properties of Balsa Core. 57

5.2 Change in pitch and maximum magnitude failure indices in controlling modes for various blade models at $V = 1.7$ m/s. 66

6.1 Summary of Conclusions 71

ACKNOWLEDGMENTS

I would like to thank my advisor, Dr. Michael Motley, for his support and guidance throughout this project. Thank you for being the first person at the UW to say "if you think you can do it, I will give you the chance" when I showed up at your door with a liberal arts background and no engineering prerequisites. Thanks as well to the rest of the faculty in the Civil Engineering department, especially Dr. John Stanton, Dr. Jeffrey Berman, Dr. Laura Lowes, and Dr. Jim Thomson, who were not far behind in lending their support and displaying a humbling amount of faith in my abilities. And an extra thank you to Dr. Laura Lowes, for serving on my committee.

I would also like to express my gratitude to Dr. Brian Polagye, for the use of his data, for serving on my committee, and for his enthusiastic stewardship of the Northwest National Marine Renewable Energy Center. NNMREC allowed me to see where my research fits into the bigger picture of marine renewable energy, sustaining my focus on the details of my project and inspiring me to look up from my work and keep exploring always.

Thanks above all to my friends and family, who have always believed in me and let me find my own path in my own time. I am more grateful than I can say for your love and endless support.

This work was funded by the University of Washingtons Royalty Research Fund and the United States Department of Energy under Grant No. DE-FG36-08GO18179-M001. The numerical modeling in this work was made possible through the use of advanced computational, storage, and networking infrastructure provided by the Hyak supercomputer system, supported in part by the University of Washington eScience Institute. I am extremely grateful for the backing of these organizations, without which this work would not have been possible.

DEDICATION

In memory of Uncle Jim

Chapter 1

INTRODUCTION

1.1 Motivation

The consumption of energy around the world is growing rapidly. This has created an increased demand for renewable sources of power generation, which in turn has generated a driving force for technological advancement. The sun, wind and oceans all contain vast amounts of energy, and there is a strong emerging market in sustainable methods of extracting that energy. Recently, solar and wind power technologies have been researched and thoroughly developed; however, the oceans remain a relatively untapped energy resource.

Systems that exploit the kinetic energy contained in a fluid flow to do work are not recent technology. Devices such as water wheels have been in use since they were invented in the early Hellenistic period. Hydroelectric dams are widespread around the world. However, taking advantage of the power contained in the ocean requires a step further, a step that was infeasible until recently due to the limits of modern technology. Ocean energy extraction requires systems that can survive the harsh nature of the offshore marine environment and are robust enough to avoid the need for constant maintenance. Beyond that, the deployment of such systems and the infrastructure for transmitting generated energy to the grid are both significant challenges. Recently, however, the high energy density and reliability of ocean currents have garnered increased attention for the ocean as an energy source, especially as more nations commit to aggressive sustainable energy goals. The energy resources contained in the world's oceans theoretically far exceed the current global power demand, and recent studies suggest that marine currents alone have the potential to supply a significant fraction of future electricity needs [10, 13].

Tidal currents are among the most consistent and reliable of the potential energy sources

contained in the ocean. While currents in the open ocean move at only a few centimeters per second, when constrained by topography to a narrow channel or strait the same current gains peak velocities of 2 to 3 m/s or more [20]. Better still from the standpoint of power generation, the variability of tidal energy is deterministic, not stochastic like that of wind, wave or solar power. The magnitude and direction of tidal current velocities are regular and predictable to a high degree of accuracy. Thus, the kinetic energy of the tides is both extremely potent and able to deliver power predictably to a time table, which eases the integration of tidal energy into existing electricity networks [68]. Yet another advantage is that tidal turbines are similar to wind turbines in operation and design, both extracting energy from the surrounding flow. This provides the nascent technologies of the tidal energy field with decades of applicable research and experimental data to inform new studies.

Though there are many benefits to marine current energy extraction, tidal turbines face significant challenges. Blade design is a critical factor in the implementation of marine hydrokinetic (MHK) turbines, as they must withstand the large, dynamic fluid forces inherent to the marine environment. A similarly-rated tidal turbine can produce four times as much energy per year as a wind turbine of the same size due to the much higher density of the surrounding flow, but this greater yield comes with an increased in drag and hydrodynamic loading [84]. Maintenance needs are considerably harder to address for underwater turbines purposefully placed in locations of extreme current, and the slender blades are vulnerable to damage by marine debris [5]. An additional concern specific to marine turbines is fluid cavitation, which can cause performance decay, vibrations, and increased turbulence. All of these obstacles underline the need for a turbine uniquely suited to its harsh environment and able to operate for long periods of time without maintenance.

Most MHK turbine blades are constructed from fiber reinforced polymer (FRP) composites. Composite materials provide excellent strength-to-weight and stiffness-to-weight ratios, improved fatigue resistance and damping properties, and can be easier to manufacture in complex shapes compared to traditional metallic alloys. Further, the anisotropic nature of these materials can be exploited by hydroelastically tailoring the design to improve performance over the expected operational life, notably in spatially varying or off-design flow conditions. This can create additional complexity in the turbine blade design problem, as

changing the material layup of the composite laminate can change the overall hydrodynamic response of the system; however, through proper design, the intrinsic bend-twist deformation coupling behavior of anisotropic composites can be utilized to develop a rapid, passive pitch adaptation, where the elastic deformations are tailored to dynamically vary with the loading condition. These fluid-structure interaction (FSI) designs have the potential to improve system performance by increasing lifetime energy capture, reducing hydrodynamic instabilities, and improving efficiency, load shedding, fatigue life, and structural integrity.

1.2 Previous Work

1.2.1 Aerodynamics

The first research on the structural tailoring of aerodynamic systems was applied to helicopter blades and focused mainly on the reduction of vibration. As manufacturing techniques became more sophisticated and composite materials more common, groups such as Friedmann et al. [22] and Ganguli and Chopra [23, 24] studied the optimization of adaptive blades in terms of performance, vibration, stability and load shedding. Ganguli and Chopra found that aeroelastic tailoring could reduce certain blade loads by up to 60% and vibrations by up to 25% while maintaining stiffness and stability [24]. Soykasap and Hodges found significant improvements in stability during both hover and forward flight using tailored composite blades [66]. Glaz et al. conducted further optimization studies on the potential for vibration reduction and found that it is possible to reduce both high- and low-speed regime vibrations, though the source of the two modes is different [26].

Helicopter rotors and wind turbines operate on very similar principals, and it is not surprising that structural tailoring of rotor blades transferred quickly from one to the other. The concept of adjusting the blade pitch of wind turbines to adapt to incident wind loading is not new; however, the idea of exploiting anisotropic or "biased fiber" materials in the blade skin to create a passive adaptation in the blades was introduced more recently. In [32], Karaolis et al. present contrasting fiber layup schemes to introduce bend-twist and stretch-twist coupling in the blades. From research conducted at the National Renewable Energy Lab (NREL) [43–46, 71], Lobitz et al. present successive studies in passive pitch

control and suggest that there is much to be gained by using aeroelastic tailoring techniques. They found that passively pitching blades can experience reduced stresses, vibration, and fatigue loading, and in some circumstances increase energy production substantially. Lee and Flay also experimented with different material layups and concluded that passive pitch control has the ability to reduce fatigue and gravity stresses [37].

Various studies have been performed on the structural aspects of composite materials for use in aeroelastic tailoring. In another study performed at NREL [28], Griffin examines fiber orientation and fabric architectures in composite materials to determine the static strength, stiffness, fabrication costs and magnitude of bend-twist coupling. Goeij et al. also analyzed passive adaptation in composite blades, focusing on the isolation of locations of excess strain. In considering the implications on manufacturing processes, they conclude that more data is needed on the subject of fatigue of hybrid laminates with off-axis fiber orientations [19].

Most recently in the aerodynamic field, passive pitch control has been researched for use in large-scale offshore wind turbines. Liu and Gong studied different composite materials and layups in passive adaptation systems. They conclude that passive pitch blades can increase the strength and resilience of offshore wind turbines, allowing for the design of systems with diameters greater than 100 m [41]. At the NREL, Ashwill performed studies on both material and geometric bend-twist coupling. These studies indicated that passive pitch control can be invaluable to shed the large turbulent loads experienced by very long blades, lowering the cost of energy and making large-scale wind turbines more feasible [3]. FSI modeling techniques are also being developed to reduce the computational time necessary to perform optimization studies [47, 48].

1.2.2 Hydrodynamics

In many ways, the mechanics of a rotor operating in the marine environment are essentially equivalent to those of a rotor in the air. Thus advances made to helicopter and wind turbine blade technology can often inform improvements to analogous marine technologies. In this case, passive pitch control has even more to offer to marine propellers and turbines than to

their aerodynamic counterparts because of the susceptibility of hydrodynamic systems to the effects of cavitation.

Every marine structure that experiences a high relative velocity to the incident flow is at risk of cavitation. In accordance with Bernoulli's equation, an increase in the velocity of a fluid will cause a decrease in hydrostatic pressure. If the fluid is in a liquid state, any decrease in pressure beyond the vapor pressure of the fluid will force the liquid to boil, forming a multitude of small bubbles. This boiling effect is called cavitation because the bubbles that form will be carried along the stream to higher pressure areas and collapse, creating a cavity in the flow that is equalized by the surrounding liquid rushing in from all sides. The flows coming from different directions meet in the center of the cavity and produce a local area of extremely high pressure. This happens on a very small scale thousands of times per second, and where the high pressure areas impact a structure such as a rotor blade they contribute to pitting, corrosion, vibration, and fatigue [35]. Gowing et al. conducted preliminary studies which indicated that the use of bend-twist coupled composite material could reduce cavitation on hydrofoils [27].

Marine structures also experience much higher loading than those operating in air, as seawater is greater than 800 times more dense than air. In this respect, the load shedding attributes of passive pitch control have the potential to provide a great benefit to marine rotors as well. In general, there are many arenas in which the exploitation of FSI effects to create passive pitch adjustment can improve the performance and structural integrity of marine rotors.

Marine Propellers

In marine and ocean engineering, investigations into passive pitch adjustment have until now focused mostly on propulsion systems. Lee and Lin conducted a series of investigations into the design and optimization of composite marine propellers. They found that flexible composite propellers could be tailored to be more efficient over a wider range of speeds when compared to traditional metallic alloy blades [38–40]. A group lead by Young also conducted numerous numerical and experimental studies to determine the effects of composite bend-

twist coupling on the performance and cavitation of marine propellers. In [78], Young and Kinnas present a numerical boundary element method code for the analysis of unsteady sheet cavitation on supercavitating and surface-piercing propellers, an extension of the solver for partially cavitating hydrofoils put forward by Kinnas and Fine in [34]. That code is further expanded and validated in [76, 80] and [82] to a boundary element method-finite element method iterating solver to include high-speed cavitating metallic propellers with small elastic deformations. In [77] and [81], Young et al. examine the effects of material anisotropy in marine propellers in steady and unsteady flow environments. The code mentioned above is expanded to include the large nonlinear elastic deformations inherent to flexible composite blades. Numerical and experimental results show that adaptive composite propellers can provide improved cavitation performance and increased energy efficiency over their rigid counterparts when operating at off-design conditions or in spatially varying flows.

Research has also been focused on the structural properties of composite blades. Though composites offer higher strength-to-weight and stiffness-to-weight ratios and reduced life-cycle costs compared to metallic blades, composite manufacturing processes are not yet streamlined and variations in materials are common [17]. Further, there are still many unknowns in the complicated loading profile and development of material degradation due to seawater [18]. In [54] and [83], Young and Motley investigate the influence of material and loading uncertainties of composites in marine environments on the hydroelastic response, safe operating envelope, and overall reliability of composite marine propellers. In [63], Orifici et al. review advanced composite failure models with the aim of developing a material model that accurately predicts failure. Motley and Young also investigate lifetime performance and issues relating to the scaling of composite materials in [53, 55, 56]. Scaling by Mach number is determined to be the most accurate strategy for predicting stress distributions, because an equivalent material and layering scheme can be used in the model and full-scale propellers, though it does not fully capture differences due to viscous effects. Even with the uncertainties inherent to modern composites, the benefits are found to have the potential to far outweigh the drawbacks in passively adaptive blade technology.

Marine Hydrokinetic Turbines

Developments in MHK turbine design can be strongly informed by advancements in the closely related fields of wind turbines and marine propellers; however, the technologies are not directly transferable. While tidal turbines are subject many of the same loading and operating conditions as marine propellers, the variability in blade geometry and system constraints creates differences in optimal designs and requires turbine-specific design and analysis programs. Similarly, marine turbine design can borrow heavily from the wind turbine industry, but tidal turbines cannot be analyzed in the same manner as wind turbines due to the added mass and other dynamic effects of the much denser fluid [69]. Codes designed for the analysis of MHK turbines must also be capable of predicting the presence of cavitation and modeling different stall characteristics than those of rotors operating in air [7].

In that light, there have recently been many numerical and experimental validation studies to determine the best techniques for modeling the performance and structural response of MHK turbines. In [6], Barltrop et al. use blade element-momentum and linear wave theories to model the effect of wave-current interactions on the bending moments at the root of MHK turbine blades. These complicated interactions are specific to marine environments and thus these studies have no precedent in the field of wind turbines. Blade element-momentum theory is also used to solve for performance by Grogan et al. [29] and Bahaj and Batten et al. [4, 8, 9]. Nicholls-Lee and Turnock research different levels of numerical intensity in computational fluid dynamics (CFD) codes to determine the balance between the computationally expensive solutions needed to capture details of the fluid behavior and faster, more optimization-oriented approaches in [58] and [59]. Full CFD codes are used by Kim et al. in [33] to determine the loading experienced in extreme operating conditions, and a finite element method (FEM) code is applied to determine structural response. In [65], Sale et al. develop and validate a methodology for the design of non-adaptive composite turbine blades also using FEM and a comprehensive structural optimization algorithm. Young et al. present an iterative boundary element method-finite element method code for modeling MHK turbine blades in [84], expanded from the code developed for modeling

marine propellers mentioned previously.

In the evaluation of the performance and structural response of MHK turbines, several aspects have been isolated as target areas where improvement is necessary before commercial tidal energy can be a viable option. One of these focus points is turbulence. Several early marine turbine pilot programs were destroyed by turbulent forces far beyond what was expected for the site. Preliminary sensitivity analyses conducted by Milne et al. found that the longitudinal turbulence intensity is a dominant parameter influencing blade root fatigue and maximum loads [49]. This has lead to a push on one side for better current resource and turbulence assessment in potential tidal energy project locations [13, 15, 64]. Equally, there has been a demand for efficient marine turbine design that can operate in conditions of greater turbulent forces and withstand the associated increased fatigue loading [70].

Cavitation susceptibility is another limit state in modern marine turbine design [5, 72]. Reducing cavitation susceptibility would allow marine turbines to operate at more efficient tip speed ratios, as the size and speed of the rotor are presently limited by the pressure reduction caused by the speed of the blade tips. Reducing susceptibility to cavitation would also enable the use of larger turbines able to extract more energy, as the amount of power generated is proportional to the swept area of the rotor. Furthermore, a reduction in cavitation would allow the installation of turbine arrays in shallower waters where the ambient pressure in the fluid is lower. This would drastically expand the number of possible sites for tidal power generation and decrease the cost of installation and implementation, as cables could be shorter and the systems would be more accessible for maintenance. In general, cavitation resistant blades would be more robust, experiencing less vibration, pitting, and fatigue loading.

Recently, the design of bend-twist coupled composite blades has been proposed to increase the performance and structural integrity of MHK turbines. Tidal turbines stand to benefit from composite materials and passive pitch control mechanisms in many of the same ways as marine propellers and wind turbines. The higher stiffness- and strength-to-weight ratios of composites and their resistance to corrosion are all valuable properties to the durability of MHK turbines [50]. In [11], Beyene and Peffley investigate geometrically adaptive composite blades and find flexible turbine blades to be more efficient than standard rigid

blades. Nicholls-Lee et al. develop an iterative solving process for bend-twist coupled marine turbine blades and found that they produced a higher power output over a wider range of tip speed ratios when compared to a rigid metallic blade [57, 60, 61]. However, their model produced unrealistically large blade deformations and did not consider site-specific parameters.

1.3 Research Objectives

Last year, the European Union's Strategic Initiative for Ocean Energy conducted an overview of the state of the art of tidal energy as well as an assessment of potential cost of energy reduction opportunities. They conclude that "There is scope for improvement in design to increase reliability and improve performance by improvements in blade design and innovative use of materials" [67]. This work addresses that area for improvement by exploring the potential benefits to be realized by using bend-twist coupled composite blades to create a passive control mechanism in MHK turbines.

While passively adaptive blades have been shown to improve MHK system performance, there are significant practical concerns that make the design of these devices highly complex. Many of the theoretical performance improvements attributed to passive control are constrained by limitations on various system components and dictated by local, site-specific operating conditions. Further, because passive control is developed through load-dependent deformations, the degradation of the material stiffness will change the FSI behavior of the system over its expected operational life and must be considered. To that end, the objective of this work is to examine the capabilities of passive pitch adaptation under both instantaneous and long-term variable amplitude loading to more fully describe potential benefits, while considering practical design and operational restrictions.

The work presented here elaborates and expands on research and conclusions which have been published previously in journal contributions and conference proceedings, namely [51] and [52].

Chapter 2

METHODOLOGY

2.1 Fluid-Structure Interaction Modeling

In order to predict turbine response, modeling of the fluid-structure interaction (FSI) effects that cause load-dependent deformation of the blade is essential. To this end, turbine blades are modeled with a previously developed and validated, fully coupled boundary element method-finite element method (BEM-FEM) solver [53, 76–78, 82, 84]. The solver begins with the undeformed blade geometry and a velocity profile in the plane of blade rotation. The BEM code uses that information to solve for hydrodynamic loading on the blade, which is then passed to the FEM code to solve for blade deformation, and that is returned to the BEM code to find an updated load profile. The process iterates until reasonable convergence is reached. A more detailed overview of the formulation and implementation of the solvers are contained in the sections below.

2.1.1 Boundary Element Method

The BEM solver of the coupled pair is a low-order, 3-D potential-based boundary element code called HE-PROPCAV [79]. PROPCAV was originally developed for the analysis of fully-wetted marine propellers in steady flow, and has been extended to model marine turbine blades and to consider the effects of spatially varying inflow, surface piercing, free surface effects, and unsteady sheet cavitation on both sides of the blade surface. Because PROPCAV was only recently adapted for the analysis of turbine blades, it introduces an extra simplification in the fluid model, namely that the axial and angular induction factors due to the blockage and wake that a turbine creates in the flow are not considered. This causes the code to overestimate power and thrust coefficients, but because this work is a comparative and not quantitative study, the simplification should not affect the conclusions drawn. This aspect of the model will be addressed in future studies.

PROPCAV solves the incompressible Euler equations in a blade-fixed rotating coordinate system. The turbine (and thus the coordinate system) is assumed to be rotating at at constant angular velocity ω. The effective inflow velocity, $\mathbf{V_e}$, is taken as the sum of the inflow in the absence of the turbine and the vortical interaction between the turbine and the inflow, or the total velocity minus the turbine-induced velocity from potential flow theory, and is defined in the non-rotating coordinate system. At a given location, $\mathbf{x} = (x, y, z)$, in the blade-fixed, rotating coordinate system the total velocity, $\mathbf{V_t}$, is expressed as the vector sum of the inflow velocity directly upstream of the turbine, $\mathbf{V_{in}}$, and the perturbation velocity potential, $\nabla\mathbf{\Phi}$, corresponding to the turbine-induced flow field, both expressed in blade-fixed coordinates. The inflow velocity, $\mathbf{V_{in}}$, can be further decomposed into the effective wake velocity and the blade rotational velocity as shown below.

$$\mathbf{V_t} = \mathbf{V_{in}} + \nabla\mathbf{\Phi} \tag{2.1}$$

$$\mathbf{V_{in}} = \mathbf{V_e} - \mathbf{\Omega} \times \mathbf{x} \tag{2.2}$$

where $\mathbf{\Omega}$ is the turbine rotational speed vector $[0, 0, \omega]^T$. The perturbation flow can be assumed to be incompressible, inviscid and irrotational.

The momentum equation with respect to the rotating blade-fixed coordinate system can be expressed

$$D\mathbf{V_t}/Dt = -\nabla P/\rho + \mathbf{g} - \mathbf{\Omega} \times (\mathbf{\Omega} \times \mathbf{x}) - 2\mathbf{\Omega} \times \mathbf{V_t} \tag{2.3}$$

where P is the hydrodynamic pressure, ρ is the fluid density, and $\mathbf{g}$ is the gravitational acceleration. The last two terms are the centrifugal acceleration ($-\mathbf{\Omega} \times (\mathbf{\Omega} \times \mathbf{x})$) and the Coriolis acceleration, or conservation of angular momentum ($-2\mathbf{\Omega} \times \mathbf{V_t}$), respectively.

By integrating the inviscid incompressible momentum equation between two points along a streamline and applying the continuity equation $\nabla \cdot \mathbf{V_t} = 0$, the following equation for the absolute total pressure P_t can be derived [76]

$$P_t - P_0 = \rho \left[\frac{1}{2} |\mathbf{V_{in}}|^2 - \frac{\partial \mathbf{\Phi}}{\partial t} - \frac{1}{2} |\mathbf{V_t}|^2 \right] \tag{2.4}$$

where P_0 is the absolute hydrostatic pressure at $\mathbf{x}$.

The fluid problem therefore is to solve for the perturbation velocity potential $\mathbf{\Phi}$, which is governed by the Laplace equation $\nabla^2 \mathbf{\Phi} = 0$. To consider FSI effects, $\mathbf{\Phi}$ can be linearly decomposed as follows

$$\mathbf{\Phi} = \boldsymbol{\phi} + \boldsymbol{\varphi} \tag{2.5}$$

where $\boldsymbol{\phi}$ is the part of the perturbation potential due to large rigid blade deformations and $\boldsymbol{\varphi}$ is the part due to the much smaller elastic blade deformations. As both $\boldsymbol{\phi}$ and $\boldsymbol{\varphi}$ are governed by the Laplace equation, they can be reduced to boundary value problems. PROPCAV solves for $\boldsymbol{\phi}$ and $\boldsymbol{\varphi}$ using a 3-D BEM approach and applying kinematic and dynamic boundary conditions as described in [84].

The decomposition of $\mathbf{\Phi}$ allows the total pressure, P_t, to be similarly decomposed into rigid blade (P_r) and elastic blade (P_v) components as follows.

$$P_t - P_0 = P_r + P_v \tag{2.6}$$

$$P_r = \rho \left[\frac{1}{2} |\mathbf{V_{in}}|^2 - \frac{\partial \boldsymbol{\phi}}{\partial t} - \frac{1}{2} |\mathbf{V_{tr}}|^2 \right] \tag{2.7}$$

$$P_v = \rho \left[-\frac{\partial \boldsymbol{\varphi}}{\partial t} - \mathbf{V_{in}} \cdot \nabla \boldsymbol{\varphi} \right] \tag{2.8}$$

P_r and P_v are then passed to the FEM solver to determine blade deformation.

2.1.2 Finite Element Method

The commercial FEM solver ABAQUS is used for the dynamic structural analysis of the blade [1]. In the blade-fixed coordinate system, the discrete equation of motion can be

expressed as

$$[\mathbf{M}]\{\ddot{\mathbf{u}}\} + [\mathbf{C}]\{\dot{\mathbf{u}}\} + [\mathbf{K}]\{\mathbf{u}\} = \{\mathbf{F_{ce}}\} + \{\mathbf{F_{co}}\} + \{\mathbf{F_h}\} \tag{2.9}$$

where $\{\ddot{\mathbf{u}}\}$, $\{\dot{\mathbf{u}}\}$, and $\{\mathbf{u}\}$ are the structural nodal acceleration, velocity, and displacement vectors, respectively; $[\mathbf{M}]$, $[\mathbf{C}]$, and $[\mathbf{K}]$ are the structural mass, damping, and stiffness matrices; $\{\mathbf{F_{ce}}\}$ is the centrifugal force, $\{\mathbf{F_{co}}\}$ is the Coriolis force, and $\{\mathbf{F_h}\}$ is the total hydrodynamic force. Like the total pressure, the hydrodynamic force can be decomposed into rigid ($\{\mathbf{F_r}\}$) and elastic ($\{\mathbf{F_v}\}$) components, by multiplying the rigid and elastic pressures by the element shape functions and integrating over the blade surface, as follows.

$$\{\mathbf{F_h}\} = \{\mathbf{F_r}\} + \{\mathbf{F_v}\} \tag{2.10}$$

$$\{\mathbf{F_r}\} = \int [\mathbf{N}]^T \{\mathbf{P_r}\} d\mathbf{S} \tag{2.11}$$

$$\{\mathbf{F_v}\} = \int [\mathbf{N}]^T \{\mathbf{P_v}\} d\mathbf{S} \tag{2.12}$$

The hydrodynamic force from elastic blade deformations, $\{\mathbf{F_v}\}$, can be computed by applying Eq. (2.8) to Eq. (2.12) and written as follows [76, 77].

$$\{\mathbf{F_v}\} = -[\mathbf{M_H}]\{\ddot{\mathbf{u}}\} - [\mathbf{C_H}]\{\dot{\mathbf{u}}\} \tag{2.13}$$

where the $[\mathbf{M_H}]$ and $[\mathbf{C_H}]$ matrices represent the hydrodynamic added mass and damping inherent to a structure moving through a dense fluid. $\{\mathbf{F_v}\}$ can be added to the left hand side of the discrete dynamic equation of motion to produce the equation in its final form

$$([\mathbf{M}] + [\mathbf{M_H}])\{\ddot{\mathbf{u}}\} + ([\mathbf{C}] + [\mathbf{C_H}])\{\dot{\mathbf{u}}\} + [\mathbf{K}]\{\mathbf{u}\} = \{\mathbf{F_{ce}}\} + \{\mathbf{F_{co}}\} + \{\mathbf{F_r}\} \tag{2.14}$$

User-defined sub-routines are employed in ABAQUS to obtain $[\mathbf{M_H}]$, $[\mathbf{C_H}]$, and $\{\mathbf{F_r}\}$ from P_r and P_v as provided by the BEM solver. The effects of large, nonlinear blade deformations are considered by iterating between the fluid and solid solvers until the solution reaches reasonable convergence. Detailed formulations of the solution algorithm, governing equations, and boundary conditions can be found in [76, 77].

2.2 Turbine Design Considerations

2.2.1 Control Mechanisms

Active Control

Traditional horizontal axis wind and marine hydrokinetic turbines fall into one of four main categories: fixed speed-fixed pitch, variable speed-fixed pitch, fixed speed-variable pitch, and variable speed-variable pitch. These categories correspond to different methods and levels of active control that affect the performance and power generation of the turbine. Because the output of each turbine is necessarily limited to the rated (maximum) power of the attached generator, some sort of active control is generally required to reduce the load on blades and generator in extreme operating conditions. Active control is also used for various other reasons, including the prevention of cavitation along the blades and, in some locations, halting the rotation of the turbine completely with the intent of minimizing interaction with sensitive marine mammal species.

A discussion of control requires working knowledge of the terminology involved. The angle of attack of a hydrofoil, α, is the angle between the chord line, a line running from the leading edge to the trailing edge of the foil, and the relative fluid velocity. The angle of attack at a point r along the blade radius, $\alpha(r)$, is a function of the blade pitch, $\phi(r)$, and the effective fluid inflow angle, $\beta(r)$, as defined below and pictured in Figure 2.1.

$$\alpha(r) = \beta(r) - \phi(r) \tag{2.15}$$

$$\beta(r) = \tan^{-1}\left[\frac{TSR}{r/R}\right] \tag{2.16}$$

where TSR is the tip speed ratio, a ratio of the speed of the rotor blade tip to the fluid velocity, expressed as TSR $= \omega R/V$. Here ω is the turbine rotational velocity, R is the rotor radius, and V is the fluid inflow velocity directly upstream of the turbine hub.

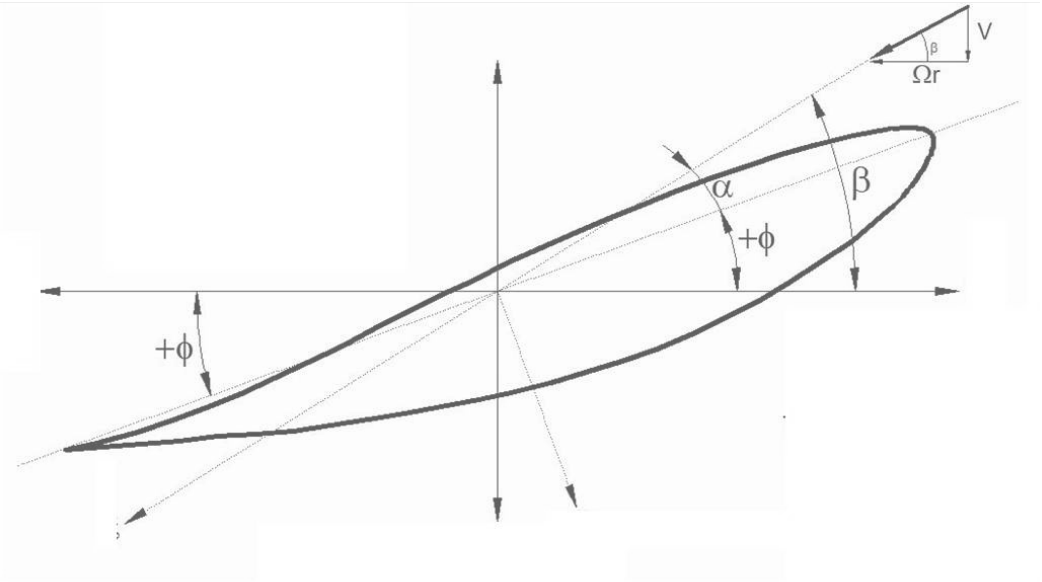

Figure 2.1: Relative angles $\alpha\,(r)$, $\phi\,(r)$, and $\beta\,(r)$.

Active control used to vary the pitch of the blades generally works by decreasing the angle of attack of each blade relative to the fluid inflow in order to decrease generated lift above rated speed, therefore slowing the rotation of the turbine. This is often referred to as an aerodynamic or hydrodynamic breaking system. In extreme circumstances, the turbine can be stopped by adjusting the blades such that the leading edge of each blade points directly into the oncoming flow and no lift is generated. On the other hand, controlling the speed of the turbine rotation uses opposite means to achieve the same effect. These variable speed turbines apply generator torque to the rotor shaft to limit the rotational speed, causing the flow over the blades to stall. Fluid stall occurs when the angle of attack of the blade becomes too large for the relative fluid velocity and the flow over the blade detaches from the top of the foil and forms turbulent eddies. This creates a reduction in generated lift which further reduces rotor speed. Stall-controlled turbines are difficult to

stop completely without imposing extreme loads on the generator, and forcing fluid stall increases the hydrodynamic loading on the blades significantly [73]. However, variable speed turbines have the benefit that a single brake mechanism in the generator is, in most cases, easier to construct and maintain than an active pitch mechanism acting in the hub of each blade. Even simpler, fixed speed-fixed pitch turbines are the easiest of the design varieties to manufacture, requiring fewest active control mechanisms. Generally, a fixed speed-fixed pitch turbine will have the ability to decouple the rotating shaft from the generator driver, allowing the turbine to spin freely in extreme conditions to avoid overloading the generator; however, this results in extremely large blade loads at high velocities. On the opposite end of the spectrum, variable speed-variable pitch systems are the most complex to design, containing both mechanical and aero- or hydrodynamic braking systems, but have the ability to reduce blade loading significantly in extreme conditions.

On average, variable speed-variable pitch turbines have the potential to generate the most power; however the associated higher initial costs and higher maintenance needs required by the active control systems can result in a higher cost per unit of electricity generated compared to simpler system designs [75]. Relative to wind turbines, active control mechanisms in MHK devices can be more costly and more difficult to control effectively. Most of the proportionally larger cost lies in the challenges of designing mechanisms for and conducting maintenance in the submarine environment. The difficulty in efficient control is due to lower maximum pitch rates and the fact that the active pitching system cannot react as quickly to changes in the inflow [74].

Passive Control

In contrast to active control mechanisms, passively controlled rotor blades are able to rapidly adjust to changing flow conditions. This creates the possibility of specifically designing blade geometries that will alter system performance by way of load-dependent deformations. Passive adaptation does not require an active driver to change the blade pitch but creates a nearly instantaneous structural response that is difficult to achieve with an active mechanism because of the high flow variation and excitation frequencies in water. One method of passive

control exploits the coupled bend-twist characteristics of composite materials. In general terms, the anisotropic nature of the composite fibers in the blade define a material strong axis that can be rotationally offset from the longitudinal axis of the blade by a specified amount. In effect, this creates a load-dependent deformation mechanism in which an applied shear load, for example, will result in twisting as well as bending deformations even in the absence of a torsional load. In this work, the degree of twisting caused by an imposed load is referred to as change in pitch, $\Delta\phi$, and the amount of bending as tip deformation, Δ.

There are two strategies to passive pitch control. An adaptive turbine blade can be designed to pitch to feather (decreased angle of attack) or pitch to stall (increased angle of attack), depending on composite laminate layup sequence. It is important to note that though the blades designed to increase angle of attack are termed "pitch to stall", they do not experience fluid stall in normal operation due to the load-dependent nature of the deformation. The name refers to the fact that an increased angle of attack pitches an airfoil *towards* stall. Because the inflow angle, $\beta(r)$, is constant for a given TSR, in order to decrease the angle of attack a pitch to feather blade must increase the pitch angle of the blade, while a pitch to stall blade will increase the angle of attack by decreasing the pitch angle of the blade.

The angle at which the fibers of each individual laminate layer are oriented defines both the direction in which the blade will pitch as well as how much the blade will deform; thus, the laminate stacking sequence is a critical design parameter for passive pitch adaptation. In practice, composite blades are composed of tens to hundreds of very fine laminate layers. Each lamina can be defined by a primary fiber angle θ from the radial axis of the blade. However, modeling each individual layer is impractical due to the high degree of computational expense, and provides a more detailed analysis than is appropriate for this stage of research. It has been shown that a multi-layered structure can be modeled using an equivalent unidirectional fiber angle, θ_{eq}, which can be found such that the effective stiffness and degree of bend-twist coupling is approximately equal to that of the full structure [42, 54, 55, 77]. The unidirectional fiber angle model need only have enough layers in the through thickness to provide the necessary mesh density for convergence, making computation vastly more efficient. θ_{eq} of a multi-layered structure can be found by means of a

composite plate analysis; in general, there are many different laminate layup sequences that will result in similar load-deformation behavior and passive adaptation and can be modeled with the same θ_{eq}. In this work, blades are modeled using a unidirectional fiber angle. While this is appropriate to determine the load-deformation characteristics and trends in the stress profile for these linear-elastic structures, detailed analysis of various multilayer models will be necessary after optimization to verify structural integrity and blade performance.

To determine performance in a unidirectional or multilayer blade model, rotor performance parameters power (C_{pow}) and thrust (C_T) coefficients are examined. Previously in the literature on wind and marine turbines and propellers, power and thrust coefficients have been presented as a function of the tip speed ratio (TSR = $\omega R/V$) for turbines or advance coefficient ($J = \pi/\text{TSR}$) for propellers. This allows for non-dimensionality on both axes and the ability to draw comparisons between studies and experiments over different ranges of inflow velocity or rotational speed; i.e, fast moving rotors in fast flows can easily be compared to slower moving rotors in slow flows because the tip speed ratio will be similar or the same. This kind of comparison does not fully capture Reynolds number effects, which compare inertial forces to viscous forces and depend on relative length, velocity, density and viscosity; however, in most cases it is a reasonable simplification to make for realistic operating ranges and adequately represents the dependence of these performance parameters. For passive pitch devices, however, other factors must be taken into account. Due to the load-dependent nature of the blade deformations, performance is not dependent solely on TSR but on the magnitudes of the inflow velocity and the rotational speed of the rotor and thus the total dimensional blade loads. As shown in Figure 2.2, if TSR changes only as a function of rotational velocity (ω) the adaptive turbine will perform differently than if TSR changes only as a function of inflow velocity (V). As such, it is critical to be able to predict and consider the deformation responses over the full range of expected site-dependent, practical operating conditions to achieve an accurate prediction of turbine performance. Each turbine is operating in a unique environment with a defined inflow velocity range and limitations on rotational speed specific to the generator system of the turbine. These parameters must be taken into account in order to create a complete picture of the structural response and thus the performance of the turbine.

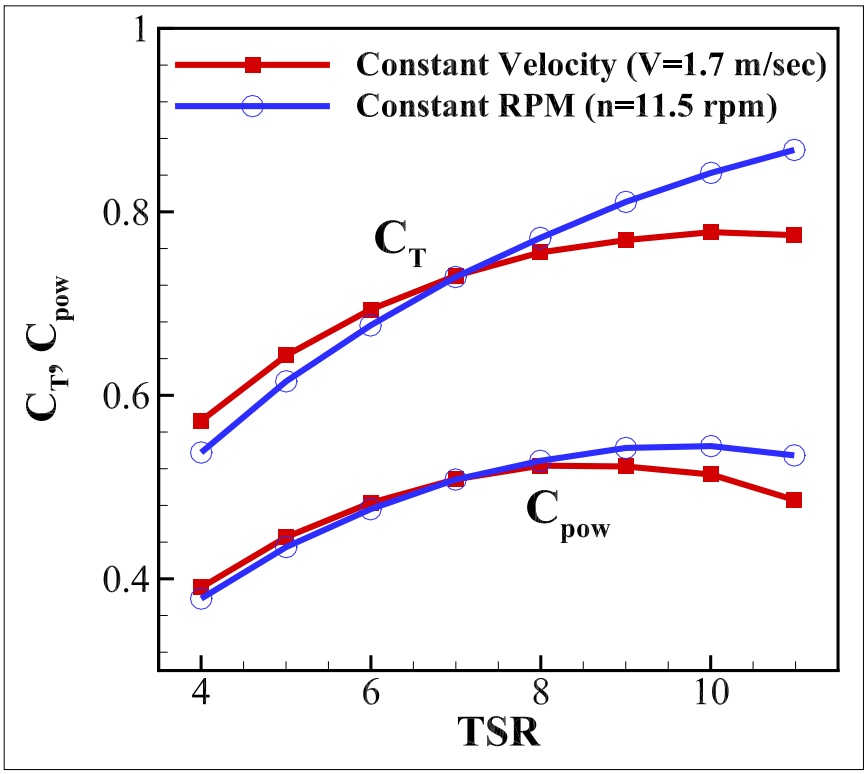

Figure 2.2: Predicted performance of an adaptive turbine in open water flow considering changing tip speed ratio as a function of V or ω only.

The potential benefits of adaptive materials and passive control on MHK devices have been preliminarily explored, but practical limitations and design considerations have not been be properly considered [61]. Many of the predicted performance improvements found by using adaptive propeller blades were shown to be overstated when applied in practical design [55], as the comparisons were not made based on comparable thrust requirements. While conceptual performance improvements can be shown, care must be taken to make fair comparisons based on operational requirements and constraints such as limits on the power generated or rotational speed of the turbine. Fair comparisons between adaptive pitch turbines or propellers can only be made by analyzing performance as a function of inflow velocity. This requires a comprehensive understanding of the local flow environment and of the possible interactions between the blades and these flows.

2.2.2 Operational Profile

Because of the importance of site-specific velocity profile characteristics in turbine design, it is essential to inform numerical simulations with realistic inflow data. The state of technology at present indicates that only areas with peak currents of 2 m/s or more are viable sites for tidal turbine implementation. While 2 m/s (3.9 kts) is a very strong current relative to most tidal locations, some sites experience currents that exceed 8 m/s. Since thrust increases with the square of velocity and power with velocity cubed, the difference between the extreme loads and available power experienced at a 2 m/s site and an 8 m/s site suggests that optimal technology and design may be highly dependent on location [14, 21]. In that light, this work uses data from a local tidal energy study to inform velocity ranges and inflow profiles. Researchers at the University of Washington have been collecting baseline data to inform the design, siting, and permitting of a pilot scale tidal energy array in Admiralty Inlet in Puget Sound, WA [64]. A four-day sample from a 104-day stationary survey using a bottom-mounted acoustic Doppler current profiler is shown in Figure 2.3 (December 2012-April 2013). The associated average annual distribution of the depth-averaged inflow velocity, based on a probability distribution of the full 104-day sample, is shown in Figure 2.4.

Due to the constant and nearly instantaneous pitch adaptation inherent to passive control systems, they are ideal for highly unsteady loading environments where fixed geometries can become suboptimal in off-design conditions. While the velocity and direction of tidal flows are vastly more predictable than wind [75], local variations in the flow profile for any given tidal cycle are to be expected due to local bathymetry and boundary effects caused by the sea floor and water surface [68]. An example of this phenomenon can easily be seen in Figure 2.3. The predictable bi-directional nature of the average inflow is evident, with an approximate 180 degree change in the flow direction, and variations such as boundary effects from the seabed and water surface can be seen as well. Figure 2.3 demonstrates the highly dynamic nature of the instantaneous velocity profile, a profile difficult and impractical to model. For numerical simulations, boundary layer effects can be approximated with a power-law estimate of the flow velocity across the water column, as shown in Figure 2.5.

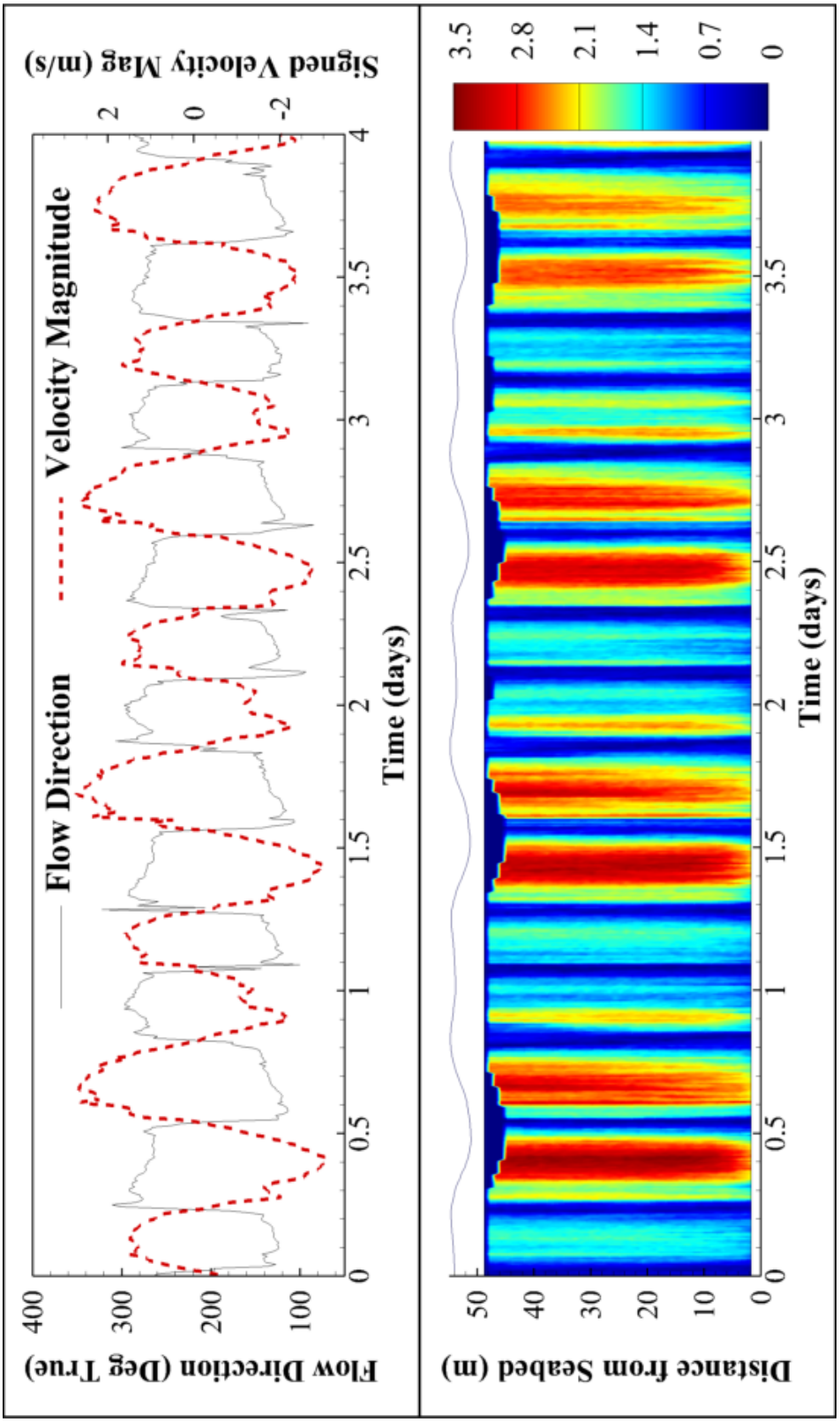

Figure 2.3: Top: measured flow direction and depth-averaged velocity magnitude data from Admiralty Inlet, WA; Bottom: measured velocity magnitude over depth from Admiralty Inlet, WA.

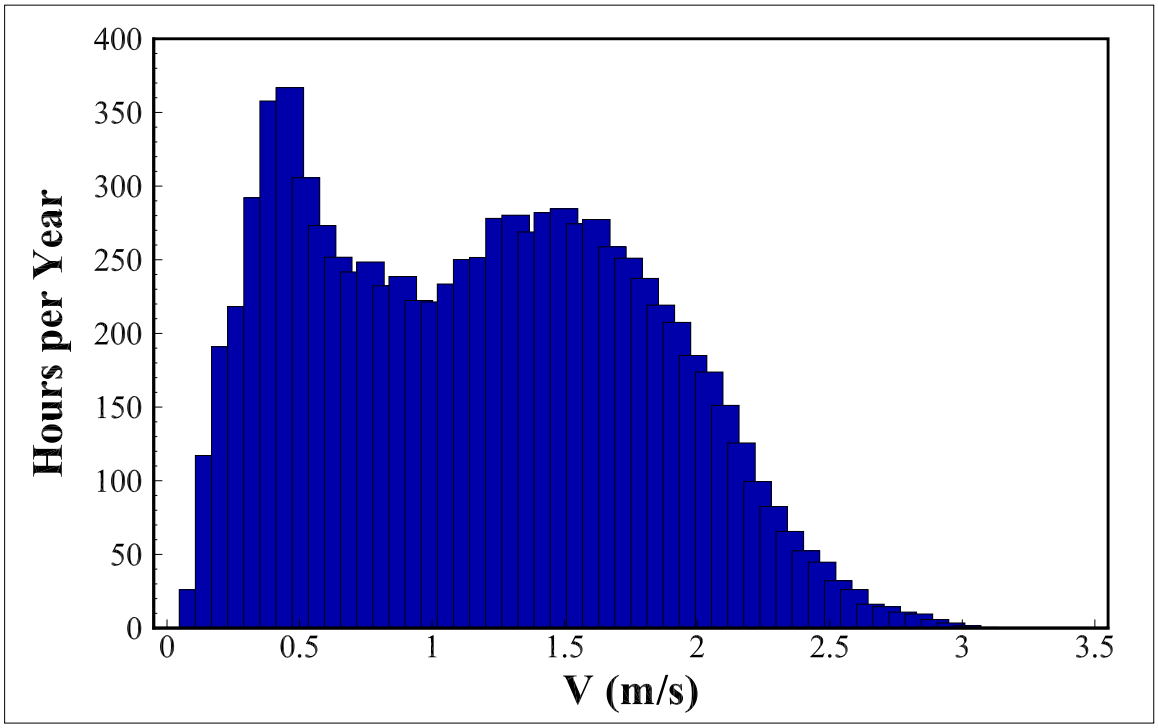

Figure 2.4: Average annual distribution of depth-averaged inflow velocities measured at Admiralty Inlet, WA (associated with data shown in Figure 2.3).

Here, a 1/7th-power law is applied, where the fluid velocity, V, at a specific height above the sea floor, h, can be defined as

$$V(h) = V_{avg}\,(h/h_0)^{1/7} \tag{2.17}$$

where V_{avg} is the mean inflow velocity in the turbine's plane of rotation and h_0 is the distance from the center of the hub to the sea floor. It is important to note that he power law is a general approximation for the mean profile and the model will likely not hold for any instantaneous profile depending on the location of the turbine in the water column and its position in the tidal cycle. Near the seabed especially, vertical shear can become a significant component of the total force on the blade. While the accuracy of the power-law estimate is

a function of location in the water column, it is adequate in this circumstance to provide a rough profile estimate that includes a representation of the variable amplitude loading that an MHK turbine blade will experience, allowing for the consideration of potential blade fatigue or other structural instabilities.

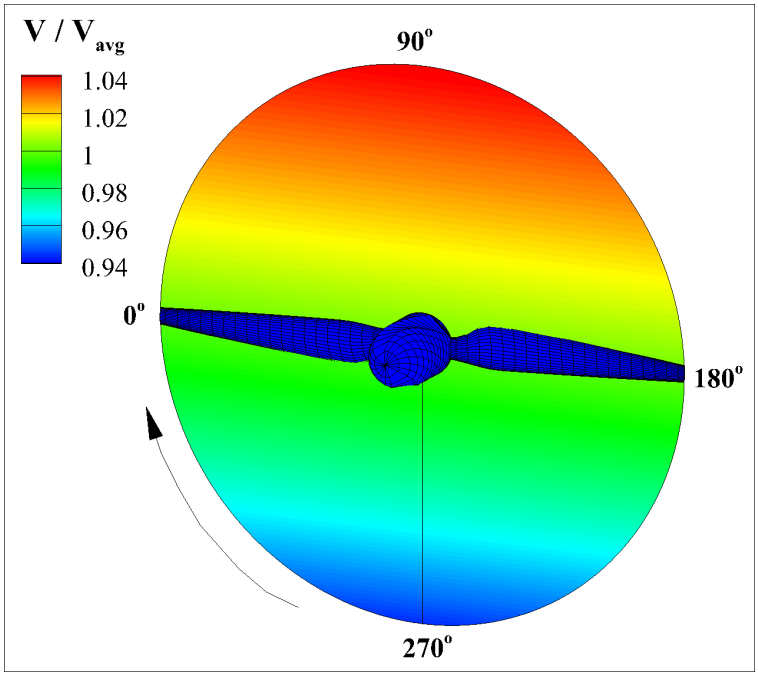

Figure 2.5: Schematic of an axial-flow turbine with a spatially varying effective inflow approximated with a 1/7th-power law.

2.2.3 Blade Model

The Department of Energy (DOE) Reference Model turbine RM1, pictured in Figure 2.6, was used for a baseline geometry in this work. The reference model is a two-bladed, variable speed-variable pitch turbine with rated (maximum) power output of 550 kW and a maximum rotational speed of 11.5 rpm to prevent cavitation. Below rated power, the tip speed ratio is held constant at TSR = 7, and above rated power active pitch control is used to maintain rated power. The turbine has a diameter of 20 meters and the center of the hub is located 30 meters from the sea floor and approximately 20 meters below the surface. The geometry

of the turbine blades is defined by the NACA $63_1 - 424$ airfoil. The NACA $63_1 - 424$ airfoil was selected due to its relatively high minimum pressure coefficient, which provides the blade with significant resistance to cavitation. The shape of the airfoil is also known to delay stall [12].

The material chosen for this research is the carbon fiber reinforced polymer Hexcel IM7-8552. The material properties are defined in Table 2.1, where the the 1-axis is defined as parallel to the fibers and the 2-axis as perpendicular to the fibers within each laminate layer [16]. In designing the blade models, the anisotropic properties of the material were oriented to produce passively controlled pitch to feather and pitch to stall blades. Further details of the reference blade can be found in [12, 36].

Table 2.1: Material Properties of Hexcel IM7-8552 [16].

$E_1 = 171.42$ GPa	$X_T = 2326.2$ MPa
$E_2 = E_3 = 9.08$ GPa	$X_C = 1200.1$ MPa
$G_{12} = G_{13} = 5.29$ GPa	$Y_T = Z_T = 160.2$ MPa
$G_{23} = 3.13$ GPa	$Y_C = Z_C = 199.8$ MPa
$\nu_{12} = \nu_{13} = 0.32$	$S_{XY} = S_{XZ} = 92.3$ MPa
$\nu_{23} = 0.45$	$S_{YZ} = 75.3$ MPa

The FEM model of the blade is made up of quadratic 3-D solid elements. Reduced integration is employed to eliminate the shear-lock failures associated with first-order elements, which causes the model to become unrealistically stiff in shear. The bulk of the model is comprised of 20-node reduced-integration volumetric brick elements (ABAQUS element C3D20R) representing the body of the blade, with 15-node reduced-integration tetrahedral elements (C3D15R) along the leading and trailing edges of the blade to accommodate the narrowing geometry [76, 80]. The nodes at the root of the blade are fixed, representing the rigid connection between the blades and the hub. The carbon fiber laminate is modeled as an orthotropic, linear elastic material with the properties defined in Table 2.1 above.

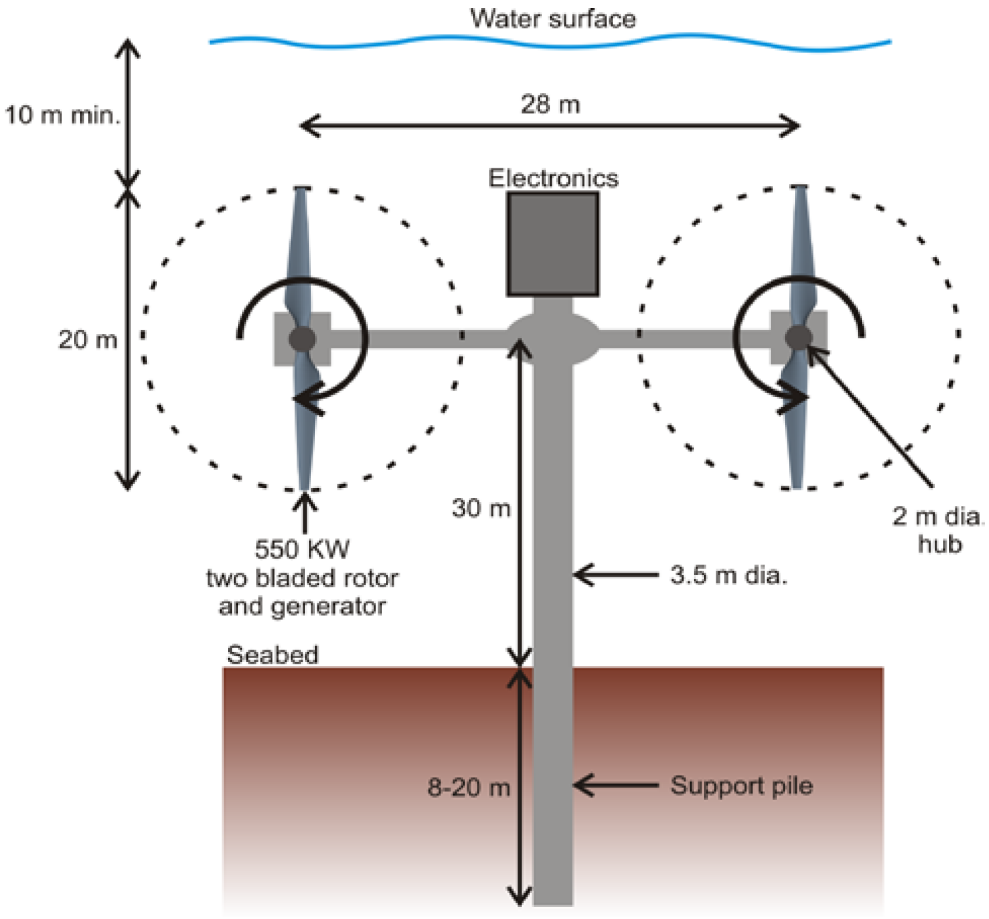

Figure 2.6: DOE Reference Model 1 [12].

Chapter 3

TURBINE PERFORMANCE

To begin the discussion of results, turbine performance is evaluated. This chapter reviews the method used to determine performance parameters, and subsequently covers the power and thrust generation of the various passively adaptive systems compared to the non-adaptive reference model.

3.1 Operating Regions

To evaluate turbine performance, it is useful to divide the operating range into three regions based on inflow velocity: zero to cut-in speed (region I), cut-in speed to rated speed (region II), and above rated speed (region III), as shown in Figure 3.1 [25]. Here, rated speed refers to the inflow velocity at which rated power is achieved. There is no power generation in region I, prior to cut-in speed, as the inflow does not provide adequate energy to overcome the inertia of the blades and the turbine does not rotate. In region III, above rated speed, rated power has been achieved and active control is necessary to maintain rated power and avoid overloading the generator system. This active control can take the form of either a mechanical brake applied to the rotor or active adjustment of the blade pitch, as discussed in Section 2.2.1. Because power output is constant by definition in regions I and III, region II is of most interest in terms of increasing turbine performance. In region II, power generated is a function of the various components of the turbine system, including the drive train, generator, and turbine blades, and thus it is this region in which any increase in power generation can be realized. Generally, such an increase will be most visible as a decrease of rated speed, meaning the turbine is able to generate maximum power at lower inflow velocities. In the theoretical ideal (in terms of turbine performance), region II would be infinitesimally small, such that rated power could be achieved as soon as there was enough energy in the flow to rotate the turbine. While this is obviously impractical, it does highlight

the conflict between performance goals and the desire to minimize the use of active control mechanisms, as active control is required in region III. Though it is noted here, this conflict will be discussed in-depth in later sections.

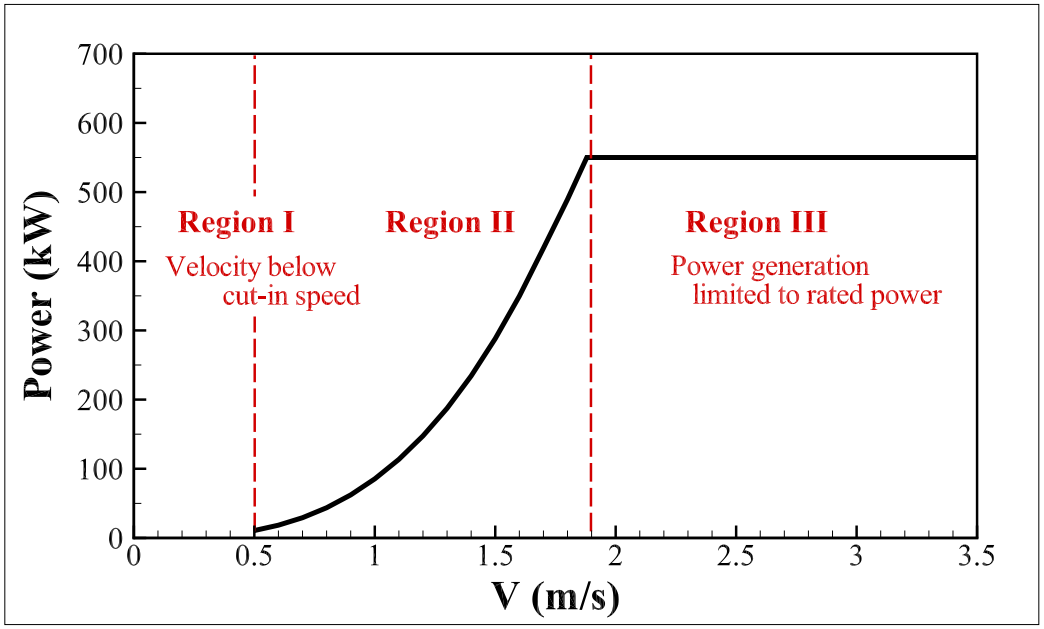

Figure 3.1: General plot of turbine power generated as a function of flow velocity.

While the shape and definition of the operating regions are independent of turbine model and location, the specific velocity and power axis labels on Figure 3.1 reflect the particular parameters of the DOE Reference Model turbine considered in this work. As mentioned before, it is essential to consider an MHK turbine in the context of a realistic setting. To that extent, it is useful to refer back to Figure 2.4, which presents the average annual distribution of the inflow velocity for Admiralty Inlet. This distribution is typical of tidal energy sites with mixed, mainly semi-diurnal tidal regimes, which experience two high and two low tides of different sizes during a lunar day, a tidal regime common to the western coast of North America. Overlying the inflow distribution data with the operating regions emphasizes the importance of turbine performance in region II. Approximately 70% of the operational life of the turbine considered in this work will be spent between the cut-in speed (0.5 m/s) and

rated speed (∼1.9 m/s for non-adaptive blades), thus any performance improvements in region II will have a significant impact on lifetime performance.

To further illustrate that point, Figure 3.2 shows a probabilistic prediction of the total amount of energy generated annually by a single turbine of this design in Admiralty Inlet, WA. Each point on the plot is determined by multiplying the amount of power the turbine can produce at any given inflow velocity (shown in Figure 3.1) by the probable amount of hours per year the turbine will be operating in that inflow velocity (shown in Figure 2.4) to display the total energy generated in each region of the operational profile. Integrating the curve gives the total annual energy production of the turbine, in this case approximately 1860 MWh. Though the turbine produces a constant amount of energy when the current velocity is above rated speed (see Figure 3.1), it spends less time operating in higher flow conditions at this site, as evidenced in Figure 2.4. Thus the shape of the curve in region III is solely a function of the rated power of the generator and the site-specific velocity distribution and cannot be improved with adaptive pitch technology. However, the energy generated in region II is dependent on the efficiency of the turbine and can be increased. As pictured in Figure 3.2, a turbine with no passive pitch adaptation generates over 60% of its annual energy yield between cut-in speed and rated speed. If the rated speed could be decreased just 0.2 m/s, meaning rated power could be achieved at inflow velocities of ∼1.7 m/s, the turbine would produce approximately 100 MWh of additional energy per year.

3.2 Analysis Method

In order to evaluate turbine performance in a site-specific manner, simulations of the reference blade and various passively adaptive blade models were run for a suite of inflow velocities informed by the Admiralty Inlet data (Figure 2.3). For this study, four passively adaptive blades are presented: $\theta_{eq} = -15°, -8°, +8°, +15°$. Negative values of θ_{eq} refer to blades that pitch to stall, while positive values of θ_{eq} represent blades that pitch to feather, as discussed in Section 2.2.1. The blade performance was simulated for inflow velocities taken at every 0.1 m/s from 0.5 m/s (cut-in speed) to 3.5 m/s (the highest velocity seen at the Admiralty Inlet site). Before the various models are compared, a brief discussion of the method of turbine performance evaluation is presented.

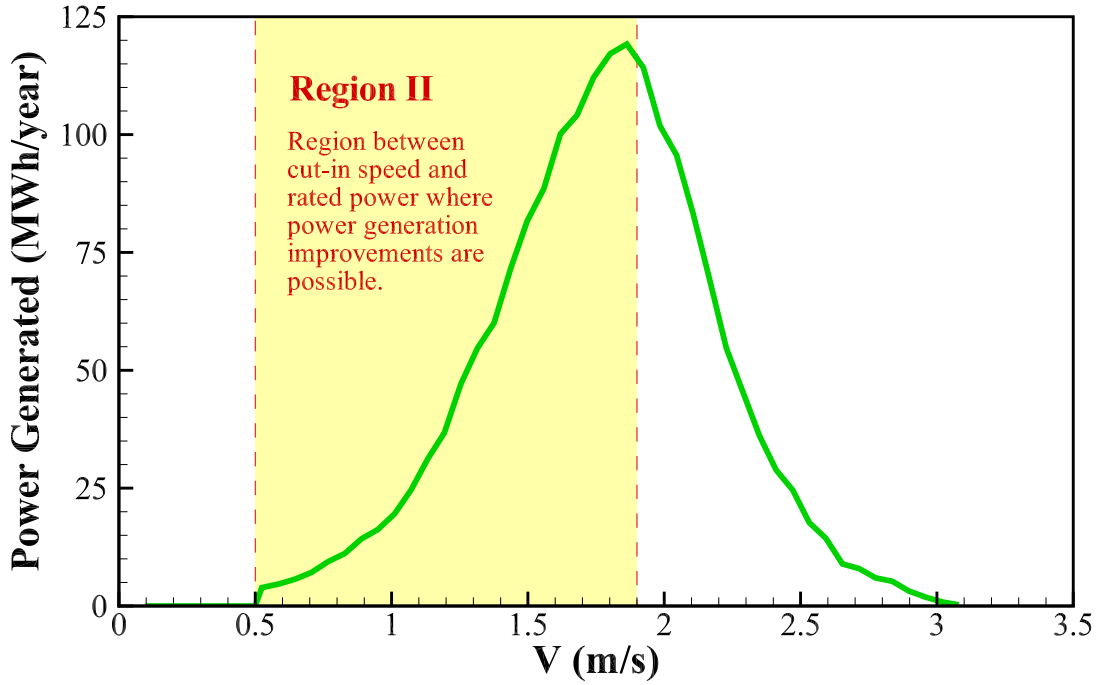

Figure 3.2: Probabilistic plot of power generated per year as a function of inflow velocity.

Turbine performance can be essentially characterized by two main parameters: the coefficients of power and thrust. The power coefficient, C_{pow}, is a non-dimensional ratio of the power extracted by the turbine to the power available in the fluid flow. Similarly, the thrust coefficient, C_T, represents the thrust on the rotor normalized by the dynamic force in the flow. The coefficients are defined

$$C_{pow} = \frac{P}{\frac{1}{2}\rho V^3 A} \tag{3.1}$$

$$C_T = \frac{T}{\frac{1}{2}\rho V^2 A} \tag{3.2}$$

where P is the power extracted by the rotor, T is the flow-generated thrust, ρ is the fluid density and A is the swept area of the turbine. These two quantities give a relative picture

of the expected power generation of the system and the amount of loading it sees. Thus, relatively higher values of C_{pow} and lower values of C_T are ideal.

Figure 3.3 presents the power and thrust coefficients for the reference, or 0°, blade. In this figure, there is a clear delineation between the region in which the turbine is operating at TSR = 7, where the power and thrust coefficients are essentially constant, and the region where the system is constrained to $\omega = 11.5$ rpm, causing both coefficients to fall in an approximately linear fashion. Another item to note is that the numerical model fails to converge at inflow velocities above 3.0 m/s. Though the power and thrust coefficients decrease as the inflow velocity builds, they do not do so drastically enough to balance out the extreme loading on the blades at higher velocities, as total thrust is proportional to V^2 and power to V^3.

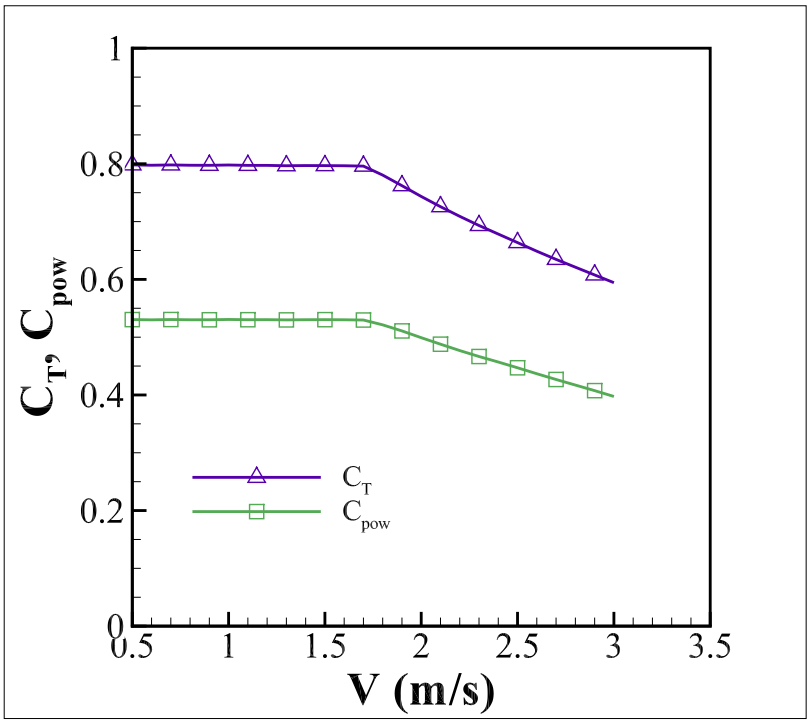

Figure 3.3: Coefficients of power and thrust for the 0° reference blade.

In order to quantitatively compare the performance of the different blade models, it is also useful to compute the full power and thrust for each system by solving for P and T in

Equations 3.1 and 3.2 above. To that end, the predicted power generation and thrust for the reference blade is shown in Figure 3.4. However, as Figure 3.4a shows, rated power must be taken into account for each blade or the power generation becomes drastically unrealistic at higher velocities. In order for the predicted performance of the blade to be representative of the constraints of the system, turbine controls that maintain rated power at higher velocities must be included in the model. Due to the fact that the reference blade does not have a passive adaptation mechanism, the undeformed blade pitch must be actively adjusted for each point above rated speed such that the power output is maintained at rated power. This active feathering of the blade mitigates the extreme loading that created the convergence failure shown in Figure 3.3, allowing the simulation to run for the full velocity range. The resulting power and thrust curves are shown for the reference blade in Figure 3.5, and the necessary active control adjustments in Figure 3.6.

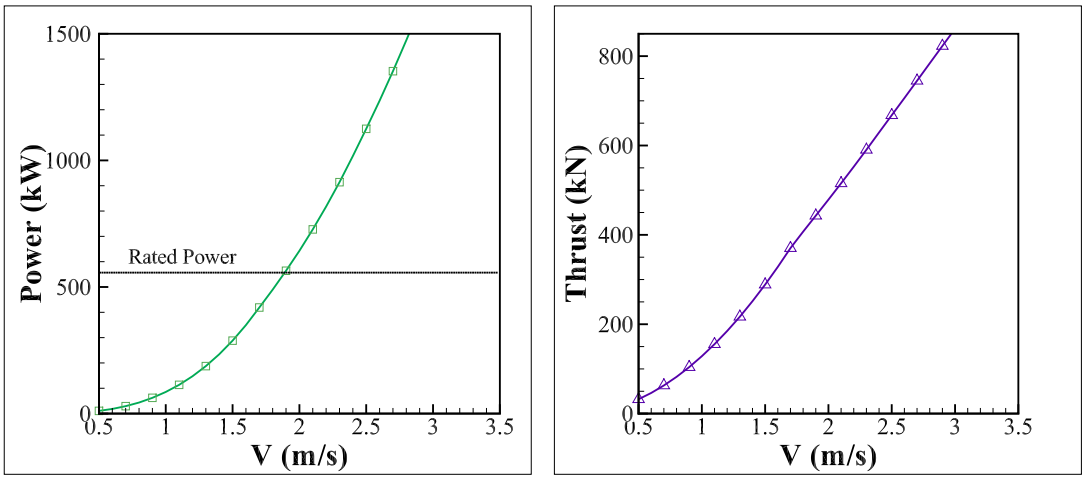

(a) Predicted power generation

(b) Predicted total thrust

Figure 3.4: Predicted performance of the 0° reference blade.

Figure 3.7 shows the impact of active control on the coefficients of power and thrust. The adjusted blades shed much of the excess loading at higher velocities, as demonstrated by the fact that the model is able to converge at the high end of the velocity range under active pitch conditions. This is a reflection of the much greater stability of the turbine when

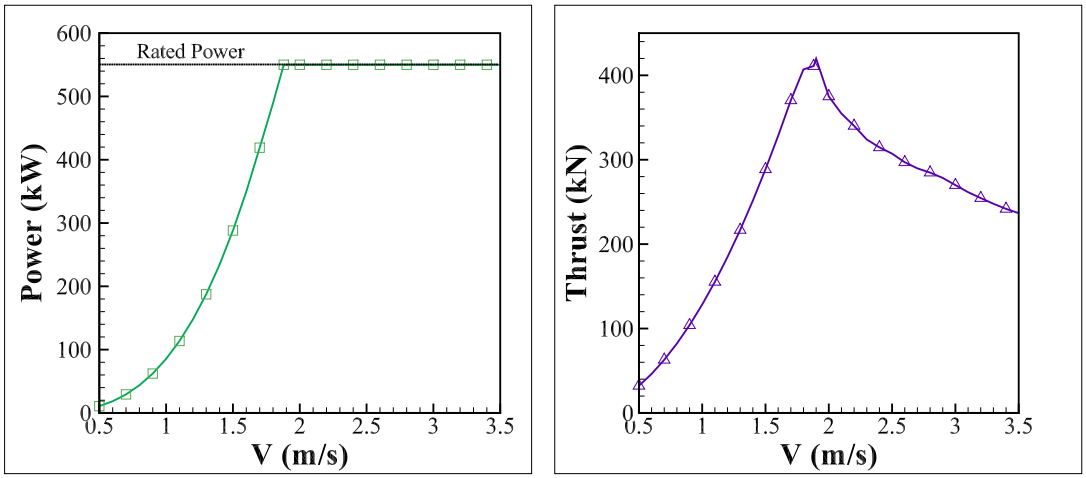

(a) Adjusted power generation

(b) Adjusted total thrust

Figure 3.5: Predicted performance of the 0° reference blade with adjustments made to account for rated power of the turbine system.

operating within practical limitations.

3.3 Performance Evaluation

The analysis method introduced above is used in this section to compare the performance of the reference blade to that of the various adaptive pitch blades. In this section, the effect of passive pitch adaptation on turbine performance is examined by comparing the power and thrust predicted for each blade configuration. Later chapters will discuss the stresses and structural response of the systems in greater detail.

To evaluate performance, Figures 3.8 through 3.11 show a comparison of the Reference Model blade (0°) with that of the passively controlled blade models, taking into account the need for active pitch. Figure 3.8 shows how the pitch of the adaptive blades changes passively with inflow velocity, depending on the equivalent unidirectional fiber angle. The angle plotted is the change in pitch at the blade tip, which is representative of the change in pitch angle distribution along the turbine blade due to the fact that the passive pitch change is effectively linear along the blade.

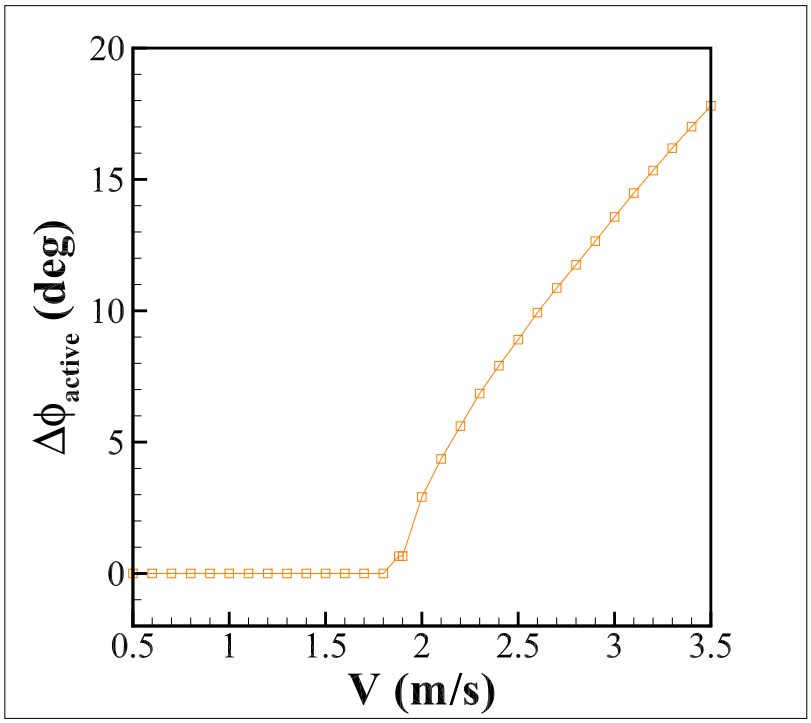

Figure 3.6: Necessary active pitch adjustment for the 0° reference blade.

As θ_{eq} deviates farther from 0°, the blade becomes more flexible and therefore the change in pitch becomes more pronounced. The distinct peak and subsequent decrease in magnitude of the passive pitch change visible in Figure 3.8 corresponds to the achievement of rated power and the onset of active pitch mechanisms, as shown in Figures 3.9 and 3.10. As the blade is actively pitched from the hub, the magnitude of passive adaptation decreases due to the relative change in inflow angle. It is interesting to note that the reference blade experiences a slight change in pitch as well. This is due to the fact that, though the fiber axis is aligned with the longitudinal axis of the blade ($\theta_{eq} = 0°$), the nature of the material and geometry of the blade still provide for some flexibility and thus the changing angle of the inflow induces a small amount of deformation.

As Figures 3.8 and 3.10 demonstrate, any change in pitch corresponds directly to a change in power generation in region II as follows:

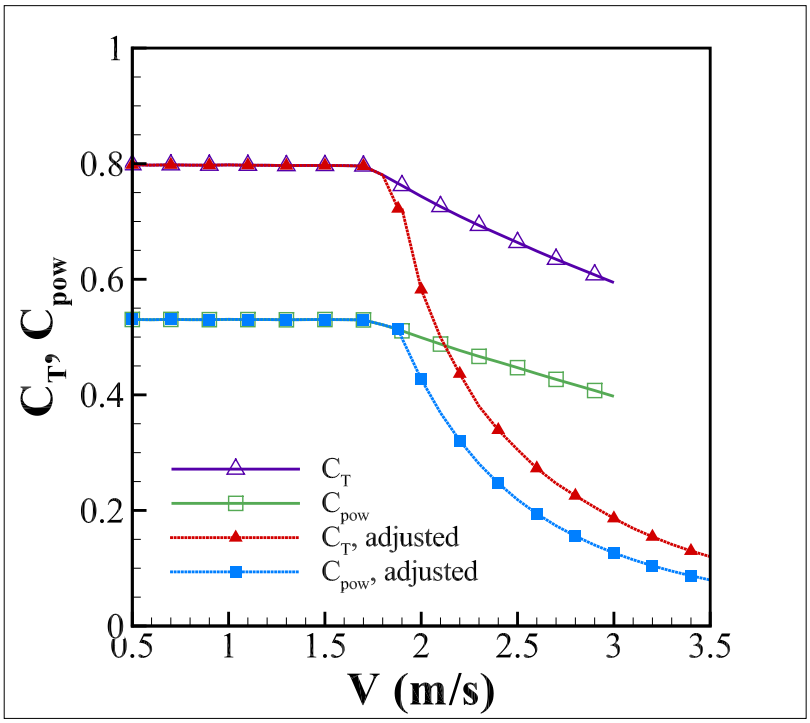

Figure 3.7: Coefficients of thrust and power with and without active pitch adjustment.

- Pitch to stall blades ($\theta_{eq} < 0$) decrease blade pitch which increases angle of attack and increases power generation as compared to the reference blade;

- Pitch to feather blades ($\theta_{eq} > 0$) increase blade pitch which decreases angle of attack and decreases power generation as compared to the reference blade.

Any increase in power comes at the price of an increase in thrust, as shown in Figure 3.11. While the structural ramifications of that fact will be discussed in the following chapters, it is worth noting the intrinsic link between power and thrust here. As power is proportional to inflow velocity cubed (P = $C_{pow} * \frac{1}{2}\rho AV^3$), thrust is proportional to velocity squared (T = $C_T * \frac{1}{2}\rho AV^2$). This leads to the intuitive increase of power and thrust in region II and also the less obvious decrease in thrust in region III, where power is held constant. When rated power is achieved, the blades are actively feathered to shed excess loads and maintain rated power. This causes the thrust on the blades (shown in Fig. 3.11) and the magnitude

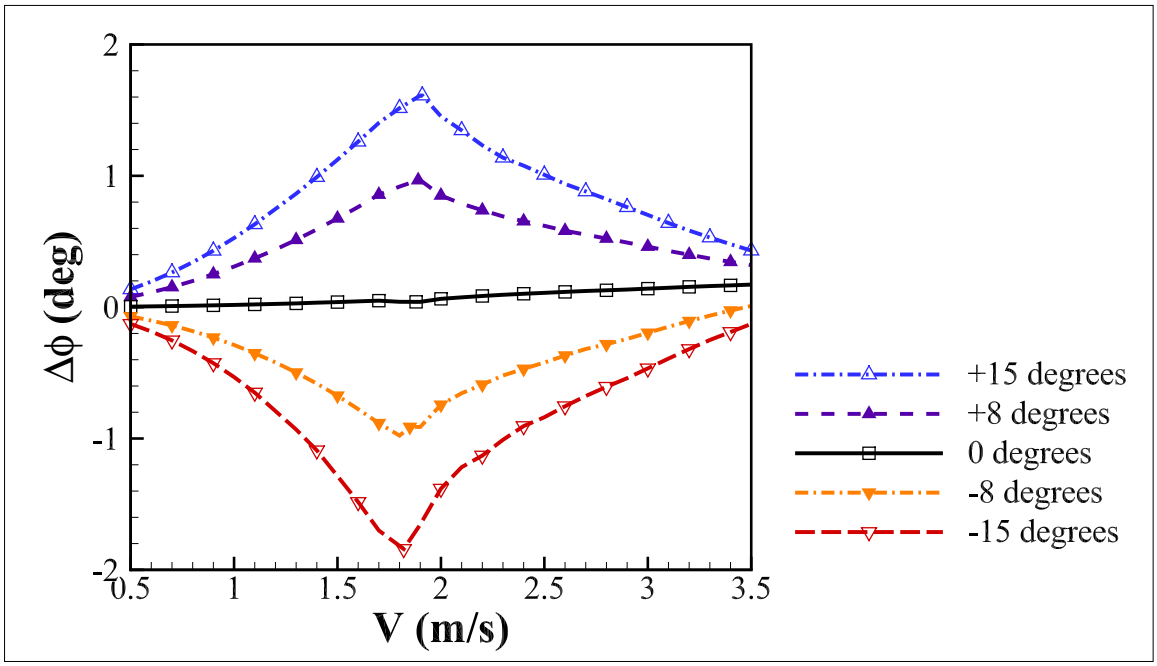

Figure 3.8: Predicted change in tip pitch angle for the reference (0°) and passively controlled turbine blades.

of the corresponding load-dependent passive pitch change (shown in Fig. 3.8) to be lower than what is experienced at the high end of region II. Beyond the rated speed, the required combination of active and passive control must be approximately the same for each blade. This is due to the fact that any turbine configuration must maintain the same rated power and the power generated is a function of the blade pitch. In this work, the blade geometry is constant and only the material properties are varied, which means the resulting thrust on the blades (Fig. 3.11) will necessarily align in region III. It is interesting to note that the maximum loads that the blades experience are not at the maximum expected inflow velocity but at the rated speed, just before the angle of attack is adjusted to maintain rated power. This will be discussed in more depth in later chapters.

Note that region II occurs prior to active pitch initiation (refer to Figure 3.9), in a velocity range where fluid stall is not a factor. The blades designed to pitch towards stall are thus able to increase lifetime energy capture. However, the price of that increase is

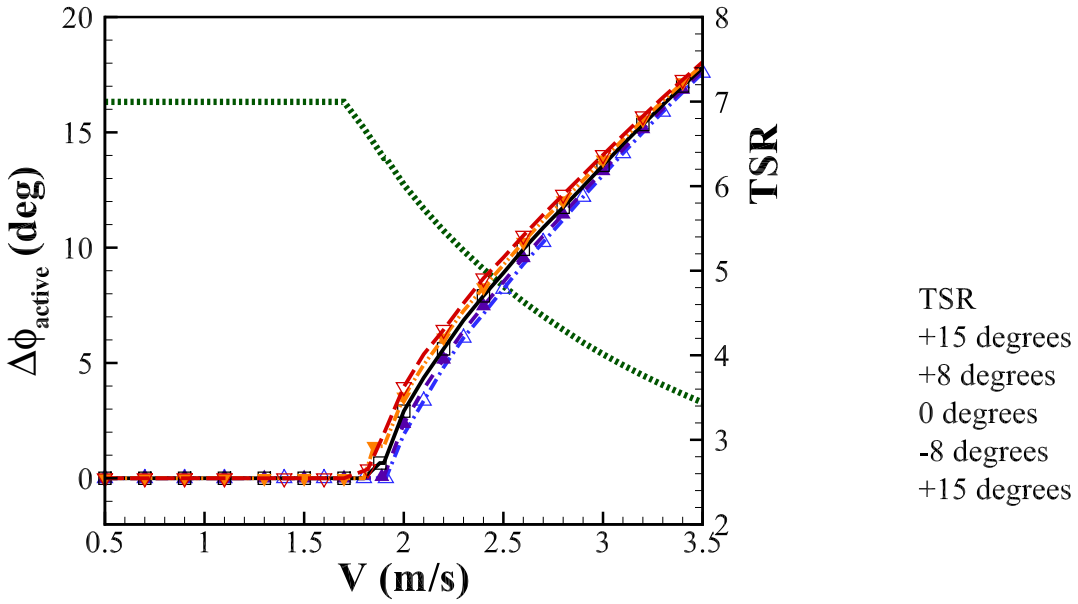

Figure 3.9: TSR and active pitch control for the reference (0°) and passively controlled turbine blades.

a corresponding increase in the thrust and an acceleration of the need for active control mechanisms, since rated power is achieved at lower velocities. As shown in Table 3.1, the amount of change in pitch is directly tied to the rated speed. While a pitch to stall blade will increase power generation, a pitch to feather blade design is required if the objective is instead to delay the initiation of the active pitch mechanism.

These preliminary studies show that the orientation of the composite fibers can be tailored to create turbine blades that pitch to stall or pitch to feather, depending on the direction of an equivalent unidirectional fiber angle from the radial line of the blade. Passively controlled blades that pitch to feather are shown to decrease angle of attack and therefore energy capture when compared to a reference blade with no passive pitch mechanism, while blades designed to pitch to stall increase angle of attack and energy capture. Those blades that increase power production were also shown to experience higher blade loads and increase the required range for active control, while those blades that decrease

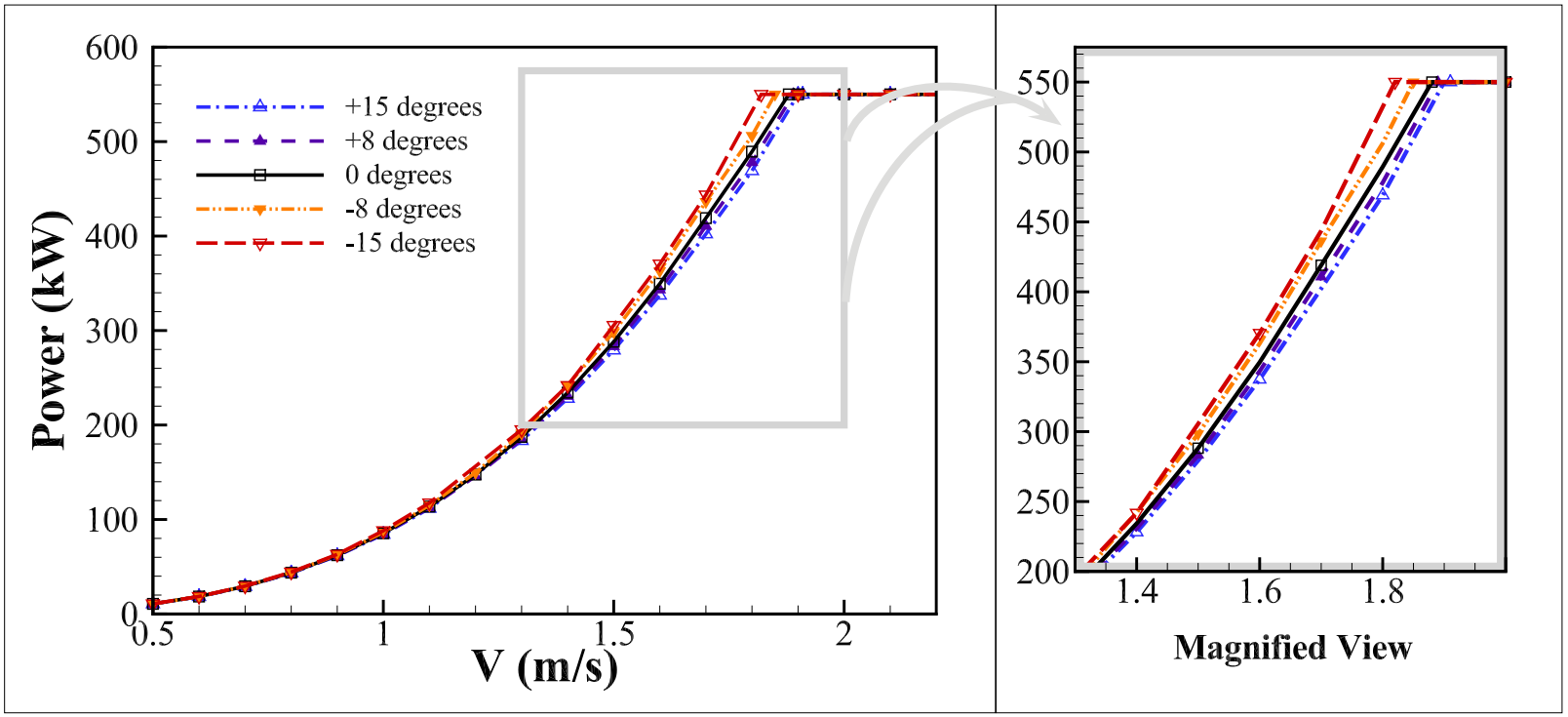

Figure 3.10: Predicted power generation of the reference (0°) and passively controlled turbine blades.

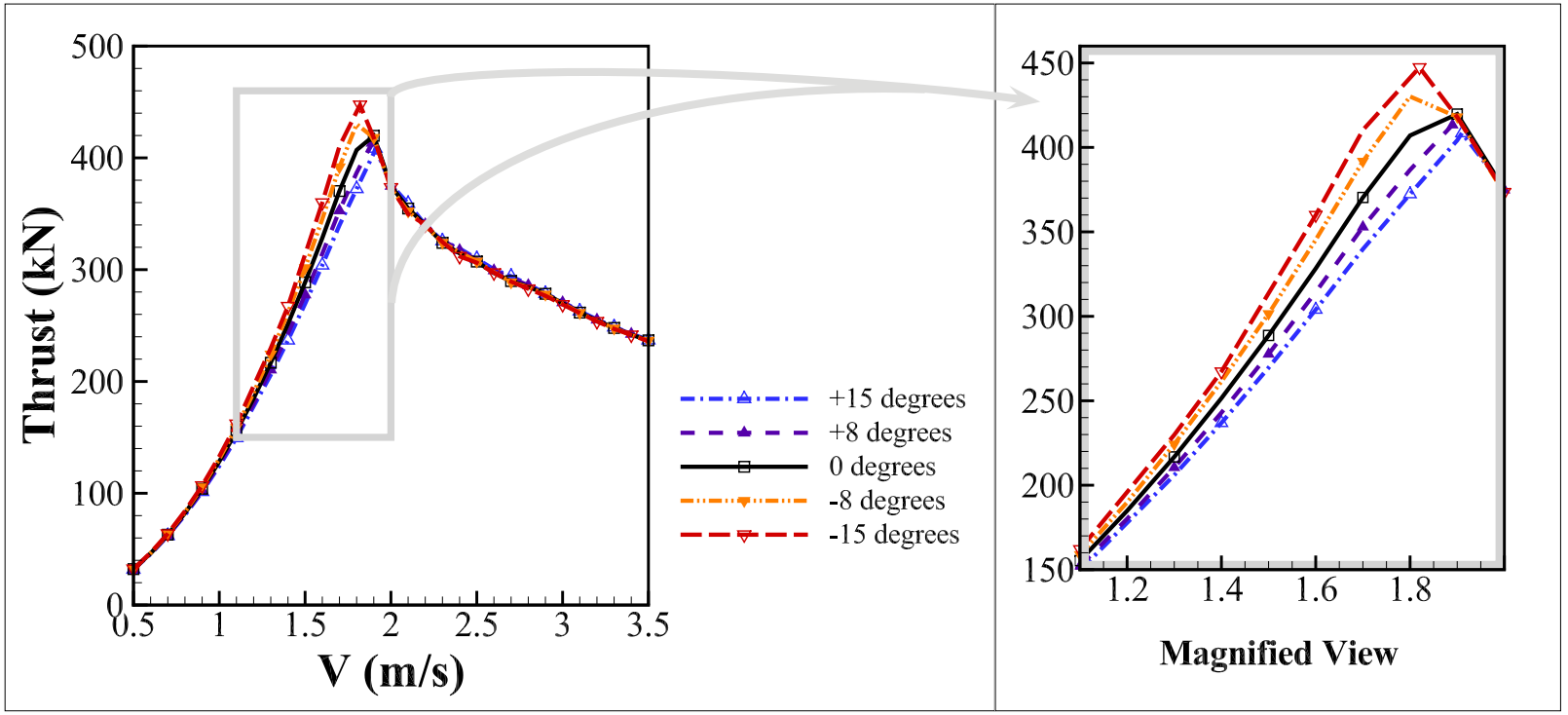

Figure 3.11: Predicted total thrust on the reference (0°) and passively controlled turbine blades.

Table 3.1: Rated speed and maximum pitch change of the various turbine blades considered.

θ_{eq}	Rated Speed (m/s)	$\Delta\phi_{max}$
-15°	1.82	1.611°
-8°	1.85	0.967°
0°	1.88	0.040°
+8°	1.89	-0.978°
+15°	1.91	-1.841°

power production were shown to result in lower blade loads and decreased active control requirements. Neither system displayed enough of a shift in active pitch requirements to suggest that a passive control mechanism could entirely replace active control, but a blade could be designed to reduce the amount of time an active control mechanism would be required.

Chapter 4

STRUCTURAL RESPONSE

To continue the discussion of results, the structural response of the adaptive blades is considered and compared to the non-adaptive reference blade. This chapter begins with a discussion of maximum blade loads and stresses, and then takes a more detailed look at stress distribution and controlling failure modes.

4.1 Blade Loads and Stresses

Assessing turbine performance is essential to estimating the power output and therefore the cost effectiveness of any potential turbine system, and many analyses of MHK turbine blades stop with performance prediction. However, performance is only one half of the picture; it is crucial to understand the structural response of the blades as well. Only in this way can the benefits and drawbacks of the system as a whole be fairly considered. To that end, the predicted blade loads and stresses are discussed here. As the plots in Section 3.3 show, however, the results of the $\pm 8^\circ$ blades trend between the $\pm 15^\circ$ blades and the reference 0° blade in all respects. These blades are therefore removed from further plots for clarity.

In Figures 4.1 and 4.2, the structural demand on the reference and passively controlled blades are compared. These figures show the maximum blade loads and the magnitude of the maximum bending stresses, respectively, associated with one revolution through the vertically-sheared inflow shown in Figure 2.5. The higher of the two lines plotted for each blade model on each figure corresponds to the maximum blade load or stress experienced at a rotation angle of 90°, where the blade is pointing vertically upwards and the velocity of the fluid is greater than the average velocity at the turbine hub. Accordingly, the lower of the two lines traces the maximum load or stress experienced at a rotation angle of 270°, where the blade is pointing vertically downwards and the velocity of the fluid is less than

the average velocity at the turbine hub. These orientations are pictured in Figure 4.3 for clarity. Note that the model turbine has only two blades, though four blades are pictured to compare the stresses at various angles.

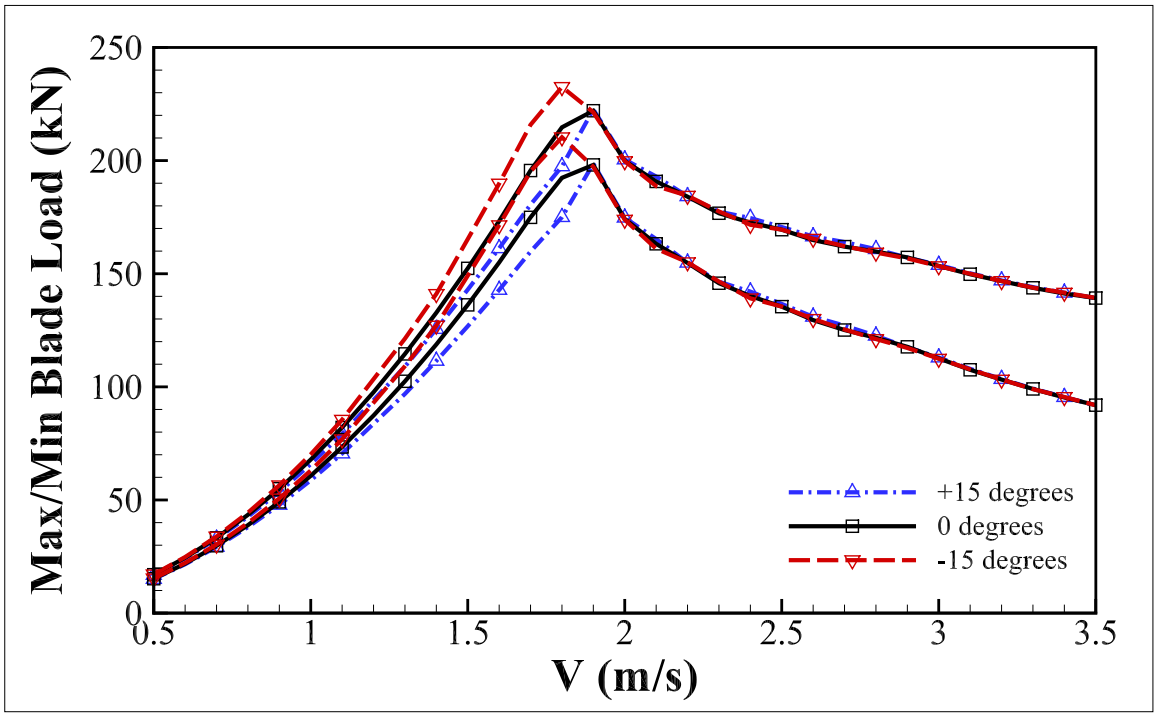

Figure 4.1: Highest and lowest maximum blade loads experienced in one rotation by the reference (0°) and passively controlled turbine blades.

As noted in Section 3.3, the thrust experienced by the turbine peaks at rated speed and then aligns at the higher inflow velocities associated with rated power for each blade configuration. The same trend is seen here in the blade load profile shown in Figure 4.1; the loading is highest at rated speed, and the loads at velocities above that point are essentially identical. There is a distinct difference, however, in the loading experienced by each blade before the initiation of the active control mechanism. As expected from the predicted thrust on the system (shown in Figure 3.11), the −15° pitch to stall blade experiences higher loads than the reference and +15° feathering blades. The loads associated with the −15° blade also peak at a fractionally lower inflow velocity, as rated power is achieved at a lower velocity

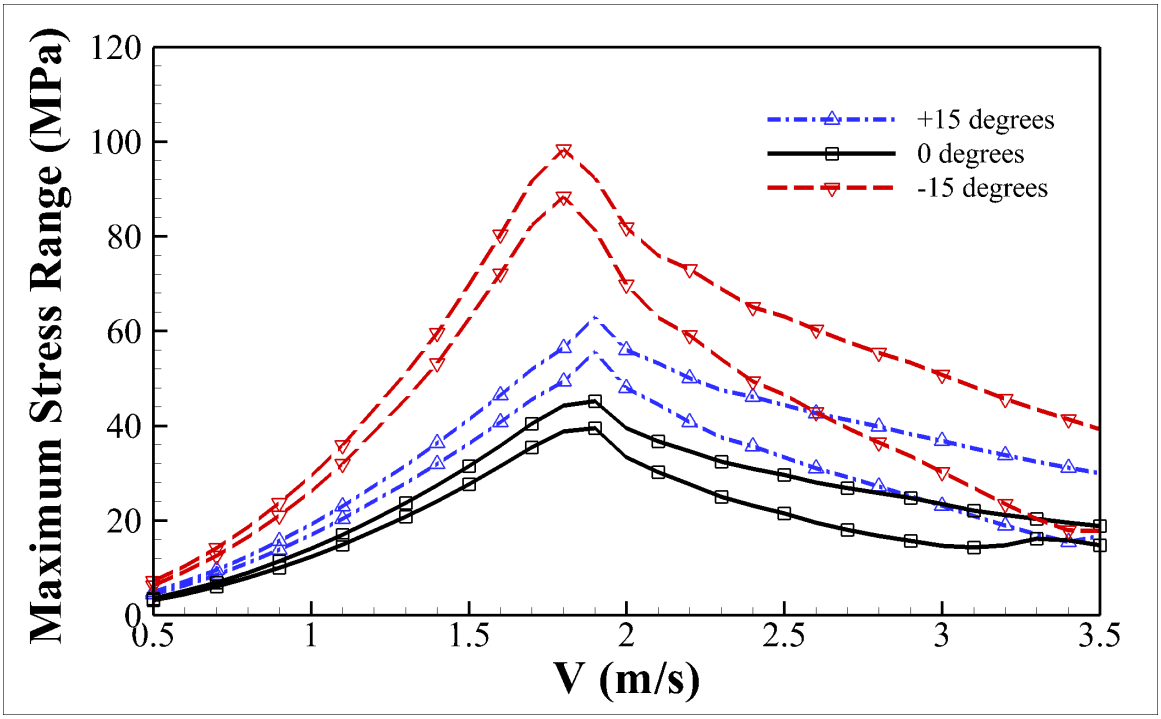

Figure 4.2: Highest and lowest maximum blade stresses experienced in one rotation by the reference (0°) and passively controlled turbine blades.

by the pitch to stall blades (see Figure 3.10 and Table 3.1). Unsurprisingly, the +15° pitch to feather blade sees the opposite effect. The feathering blade experiences lower loads than the reference and −15° pitch to stall blades, associated with the lower thrust shown in Figure 3.11. These trends correspond to the power generation shown in Figure 3.10: the adaptive pitch to stall blade both generates higher power and develops higher loads than the reference blade, while the pitch to feather blade trends in the inverse direction. Further, the maximum loads are not associated simply with the maximum inflow velocity but depend on operational requirements (i.e. active control, rotational frequency, etc.), which, for adaptive pitch blades, depend on the design of the blades themselves.

The range of maximum blade bending stresses resulting from the loads shown in Figure 4.1 are shown in Figure 4.2. Critical observations about the structural composition of passive pitch blades can be made from this figure. Like in previous figures, the highest stresses for

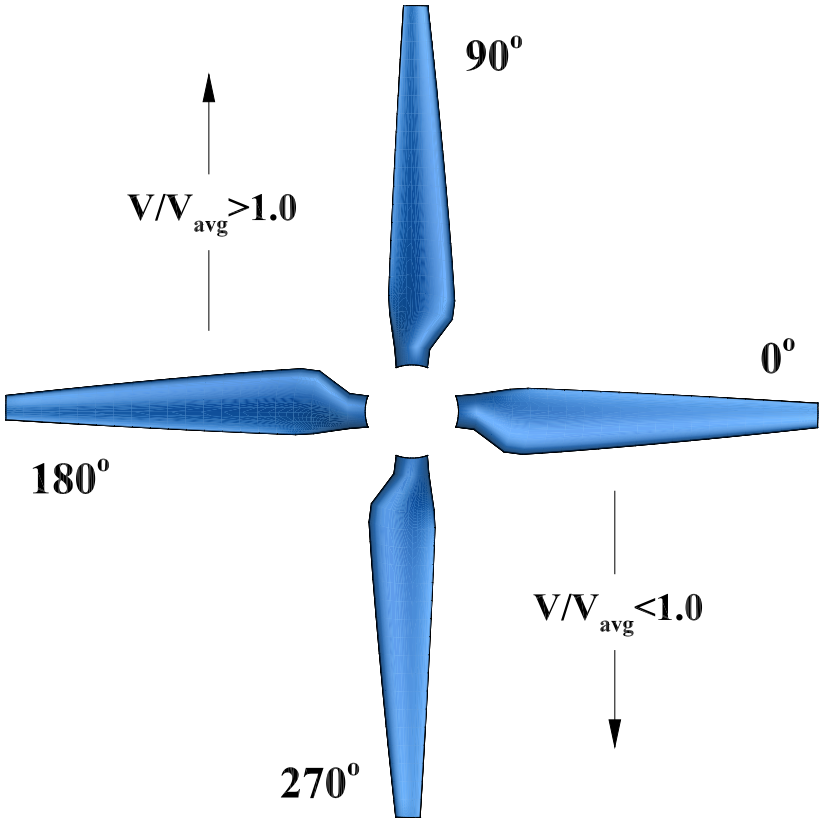

Figure 4.3: Turbine blade reference rotational angles.

each material layup occur at rated speed. However, Figure 4.2 shows two unusual features. First, contrary to previous plots, the maximum stresses seen in each of the blades are not equivalent in region III where rated power is maintained. Second, while thrust and loads on the $+15°$ feathering blade are lower than both the $-15°$ pitch to stall blade and the reference $0°$ blade, here the case is different. Though the integral of the stresses must equal the load, the maximum stresses experienced by the pitch to feather blade are higher than those on the reference blade, though still lower than the pitch to stall blade. While this may be initially surprising, both of these features can be explained by the nature of the bend-twist coupling mechanism. The increased blade stresses in the pitch to stall and pitch

to feather blades are due to the greater flexibility of the adaptive blades, which is evidenced in the magnitude of the change in pitch (shown in Figure 3.8). The stress profiles do not align at higher velocities due to the changes in primary fiber angle required for passive adaptation that create this increased flexibility in the blades. Further, even though the blades that pitch to feather experience lower blade loads, the inherent material properties and increased flexibility result in higher stresses near rated speed when compared to the reference model.

It is important to examine not only the magnitude of the maximum stresses, but also the stress distribution across the blades. For that purpose, Figures 4.4-4.6 compare the stress fields on the different blade models. Figures 4.4 and 4.5 show a contour view of the stresses on the pressure and suction faces for the pitch to feather and pitch to stall blades at various blade rotation angles; Figure 4.6 shows the bending stress contours on the pressure face of all three blade models. The comparisons are taken at $V = 1.7$ m/s, as that is just before the initiation of active control mechanisms for all models considered in this work. These figures correspond to the stresses found in the adaptive blades in Figure 4.2. The maximum stresses occur over a relatively small area of the blade face, and follow the fiber orientation of the blades. Further, the induced bending and twisting deformations in the adaptive blades lead to higher stresses, especially towards the base of the blades.

4.2 Predicting Composite Failure

In order to quantify the stresses experienced by the turbine blades in a useful way, it is necessary to compare them to some sort of composite failure index. Unfortunately, fiber-reinforced polymer (FRP) composites like the material modeled in this work are extremely complex, and it is therefore much more difficult to define failure in these composites than in metallic materials, for example. FRP composites are made of many laminate layers of woven polymer matrices strengthened by reinforcing fibers. In these materials, the development of damage leading to fatigue depends on many parameters including geometry, material, laminate lay-up, loading conditions, and load history. Furthermore, composites can display a multitude of failure mechanisms which often build up at the microscopic level and lead to a major visible failure. For the purposes in this work, the most general cases of failure will

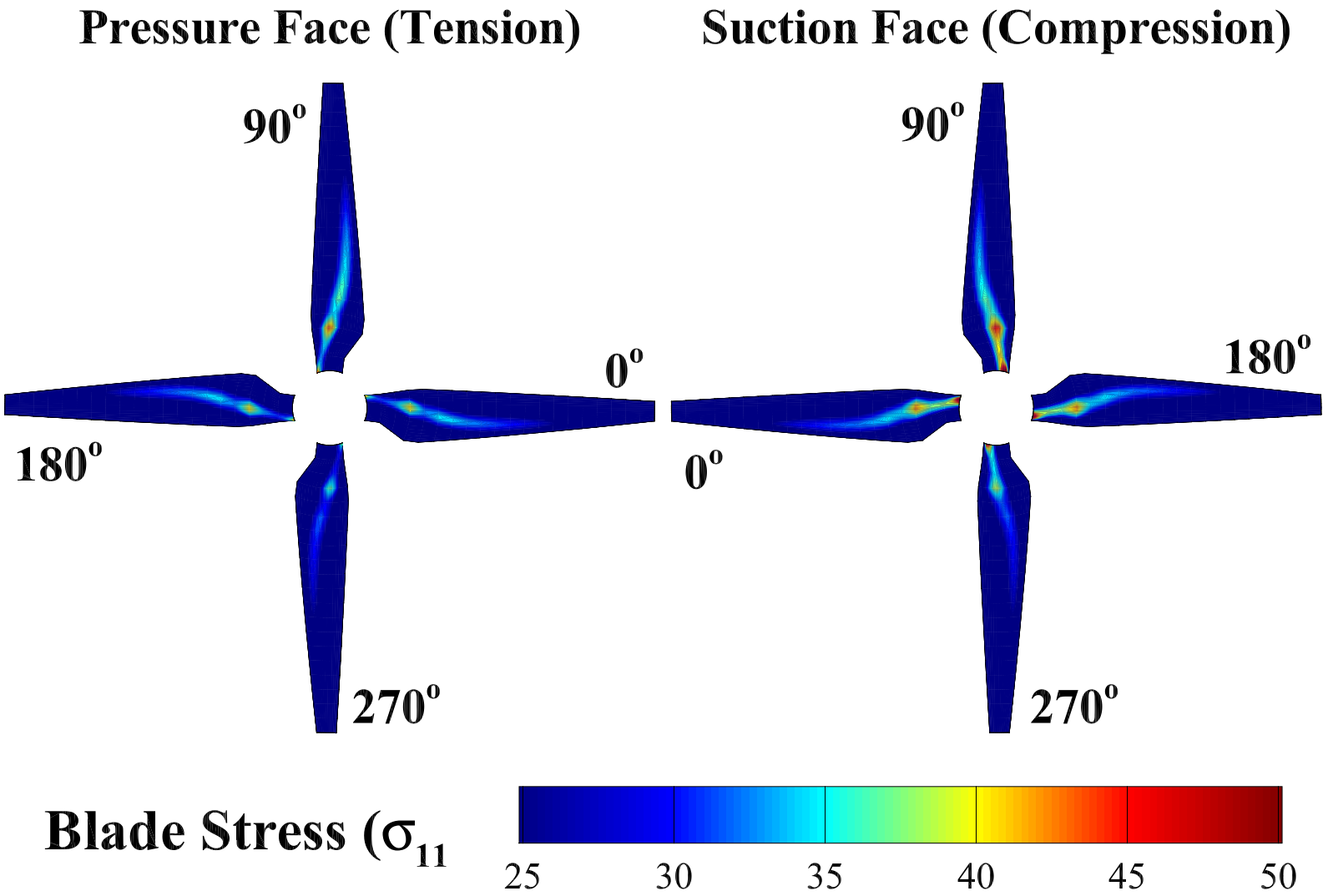

Figure 4.4: Blade bending stress (σ_1) on the pressure face (left) and suction face (right) at various blade angles corresponding to $V = 1.7$ for the $+15°$ pitch to feather blade.

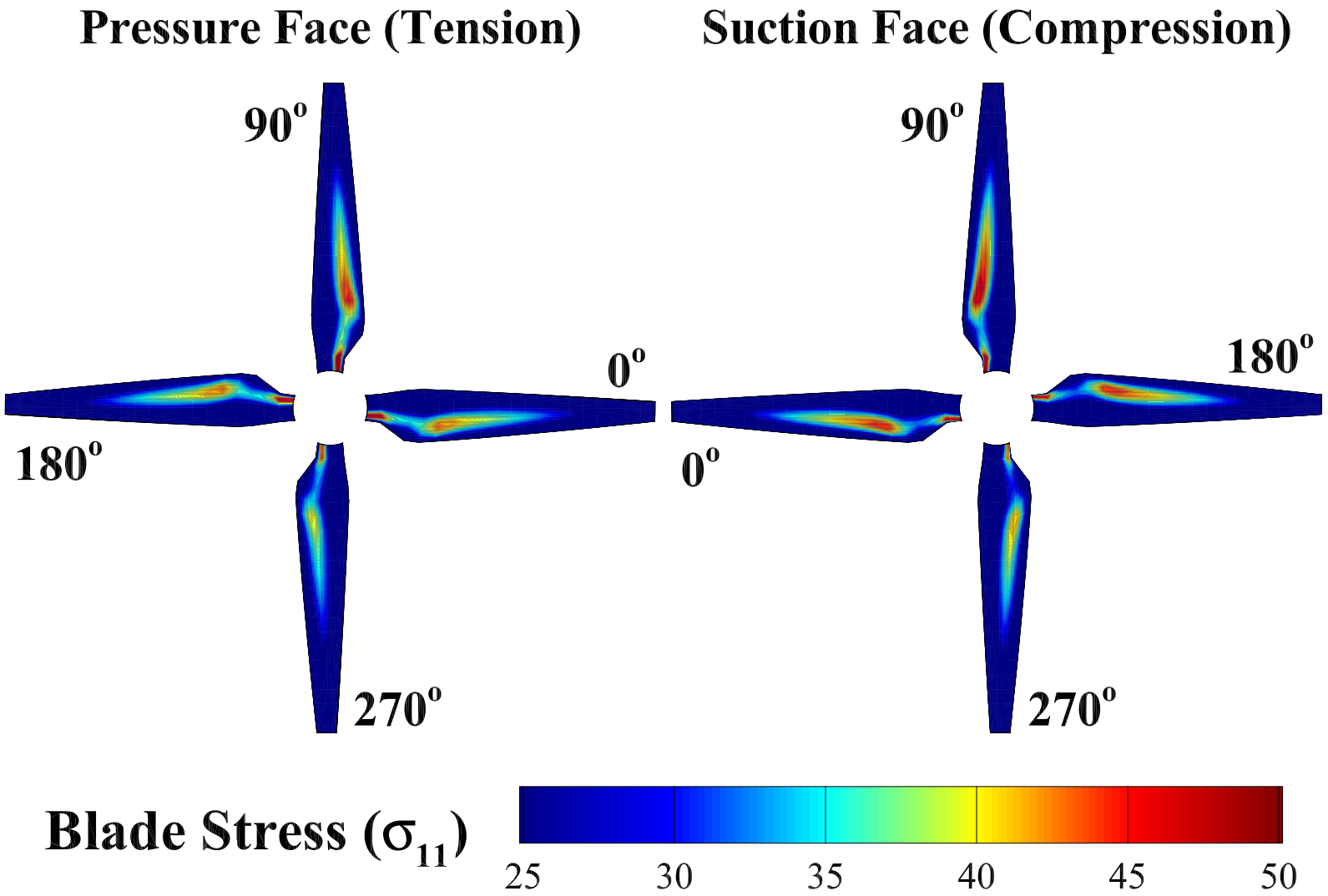

Figure 4.5: Blade bending stress (σ_1) on the pressure face (left) and suction face (right) at various blade angles corresponding to $V = 1.7$ for the $-15°$ pitch to stall blade.

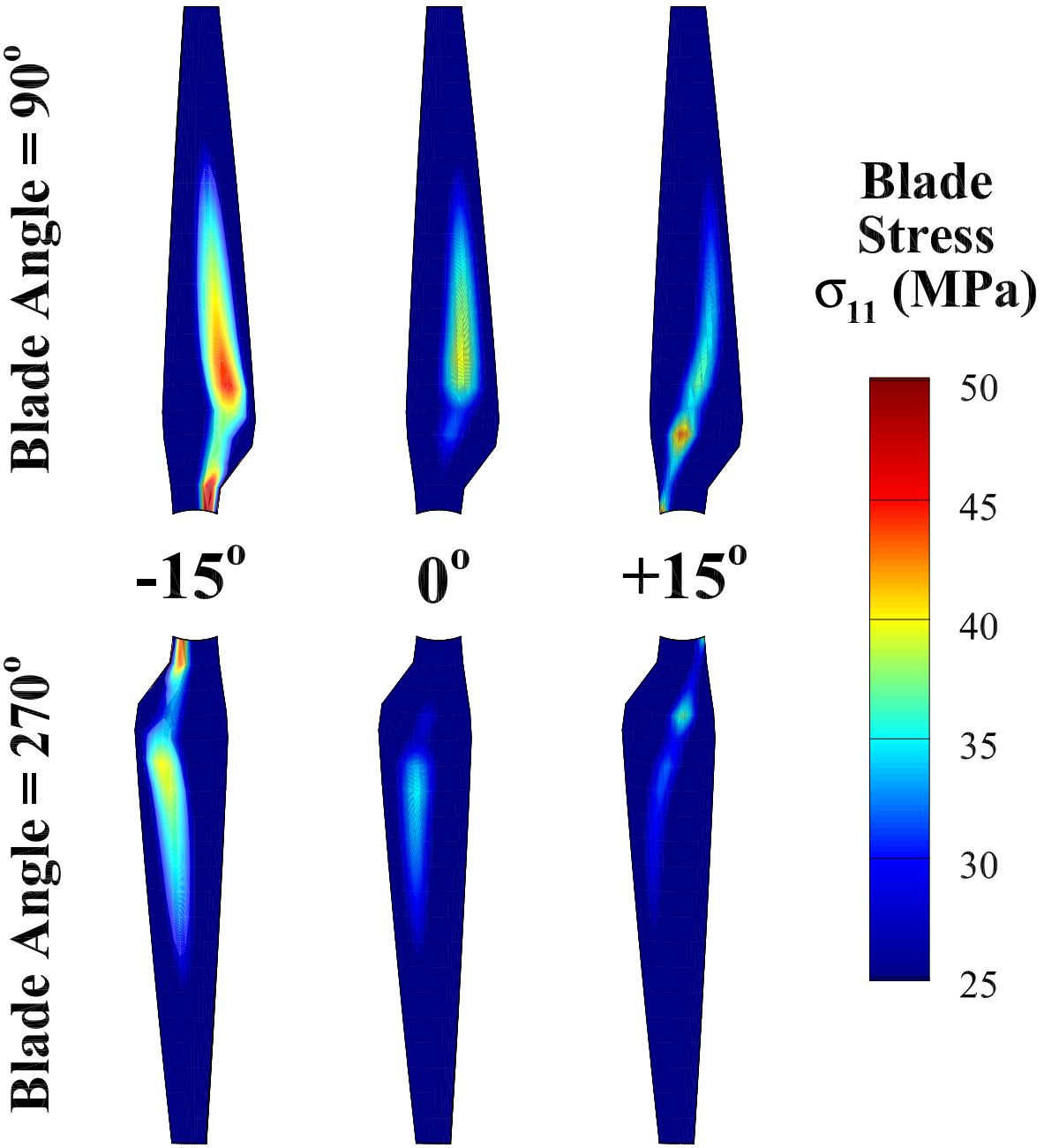

Figure 4.6: Blade bending stress (σ_1) on the pressure face for the pitch to feather ($+15°$), pitch to stall ($-15°$), and reference blades corresponding to $V = 1.7$ at blade angles of 90° (maximum load) and 270° (minimum load).

be considered, as defined below. A selection of images representative of composite failure modes are shown in Figure 4.7.

On the simplest and smallest scale side of the spectrum are failures that develop in the reinforcing fibers, along the ply fiber axis. Fiber tensile failure occurs when the loads applied to the material cause yield or fracture in the fibers. Figure 4.7a shows an example of a tensile fracture failure. Tension can also cause individual fibers to pull out of a laminate layer. In compression, fibers can crush, buckle or kink, as shown in Figure 4.7b. To define tensile or compressive failures, a generally accepted method applies a maximum stress or maximum strain limit [63]. In this work, a maximum stress criteria is used to monitor fiber damage.

The next largest scale failures occur at the matrix level, when cracks or voids form between fibers in the matrix of a single laminate layer. This type of failure generally develops in-plane and orthogonal to the fiber axis, accumulating throughout the laminate and leading to failure across a critical plane, and often propagate from material or manufacturing defects. An example of a matrix failure is shown in Figure 4.7c. A maximum stress or strain limit can be applied to quantify matrix failure, though more complicated methods are widely used as well. Both a maximum stress limit and a quadratic normal-shear interaction equation are used to determine matrix tension and compression failure indices in this work. To analyze fiber-matrix shear failures, a similar quadratic interaction criterion is used. It is interesting to note that there does not appear to be a consensus on the use of tensile or compressive strength in the denominator of the first term of this equation [63].

On the largest scale of the material, the composite layers can become detached. This is a failure mechanism known as delamination, which generally occurs due to high through-thickness stresses. There are many different standards for analyzing the initiation of delamination and its propagation; the criteria used here focuses on simply the initiation of failure, as an extended study into progressive damage modeling is well beyond the scope of this work. A simple maximum stress and a quadratic interaction limit are applied to determine the probability of delamination initiation here.

While there are many ways to quantify the development of failure mechanisms in composites, this work uses several of the most common methods to determine the mechanisms

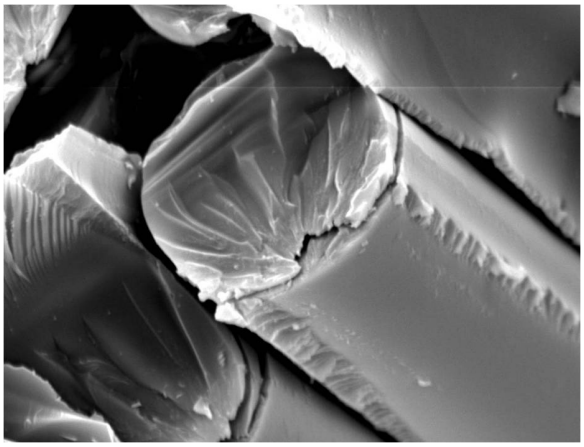

(a) Fiber Tensile Failure: Fracture [2]

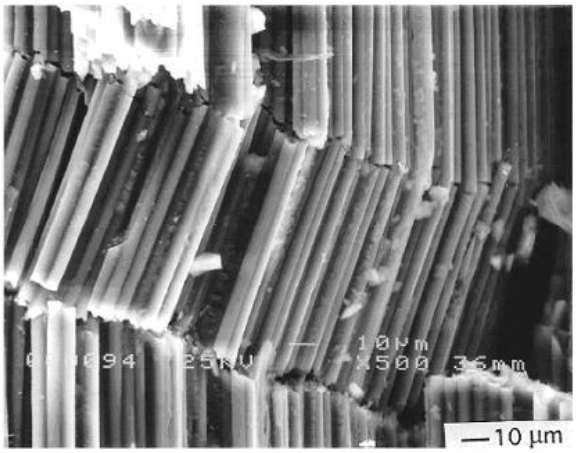

(b) Fiber Compressive Failure: Kinking [62]

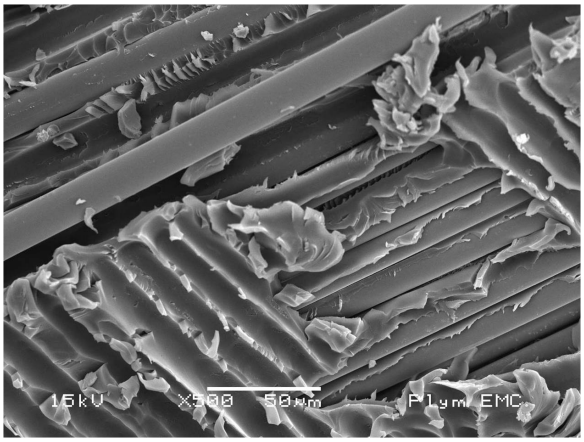

(c) Matrix Failure [2]

Figure 4.7: Examples of various composite failure mechanisms.

that introduce the highest likelihood of failure. The failure criteria used here are informed by the the work done by Hashin in [30] and Hashin and Rotem in [31], and are presented in Table 4.1. Here, σ_1 refers to the stress along the longitudinal axis of the blade, σ_2 the stress along the crosswise axis and σ_3 the through thickness stress. The strength parameters X_T, X_C, Y_T, etc. are listed with the material properties in Table 2.1.

Figures 4.8-4.10 show contour plots of the failure indices. Though all the criteria listed in Table 4.1 were examined, for clarity only the controlling modes are shown here. None of the failure criteria limits are near to being reached in any of the mechanisms; however, there are still many things to be learned from these figures. In Figure 4.8, the tensile and compressive fiber maximum stress modes are presented. On the pressure face of both blades, the tensile forces are significantly lower than the compressive forces on the blade suction faces. It is interesting to note that while the compression side stresses are close to equal in magnitude between the $+15^\circ$ pitch to feather and the -15° pitch to stall blades, the location of the maximum stresses vary considerably between the two blade models. The highest stresses occur much closer to the root of the feathering blade as opposed to near the blade center on the pitch to stall blade. The same is not true for the matrix failure mechanisms shown in Figure 4.9, where the general location of the greatest magnitude indices is the same for both sides of both blades. The pitch to stall blade in general sees higher matrix failure indices in tension and compression, with the greater magnitude indices on the suction side. However, the pitch to feather blade shows higher magnitude stresses on the tension side of the blade than the compression side. This is likely due to the difference in direction of blade twist deformation induced by the opposing adaptive material schemes. That difference is highlighted further in Figure 4.10, which shows the failure indices of the fiber-matrix maximum shear stress failure mode. The magnitude of the stresses in Figure 4.10 follow the general trend seen in previous figures, with the greater magnitude stresses showing on the -15° pitch to stall blade as compared to the feathering blade. However, the direction of the shear stresses on each blade is what makes this figure valuable. It is clear from the directly opposing shear stresses that the blades are twisting in contrasting fashions.

From Figures 4.8-4.10, it is clear that the fiber-matrix maximum shear limit represents

Table 4.1: Methods of predicting composite failure mechanisms used in this work.

Criterion	Equation
Fiber Tension, Maximum Stress	$\left\|\frac{\sigma_1}{X_T}\right\| \leq 1$
Fiber Compression, Maximum Stress	$\left\|\frac{\sigma_1}{X_C}\right\| \leq 1$
Matrix Tension, Maximum Stress	$\left\|\frac{\sigma_2}{Y_T}\right\| \leq 1$
Matrix Tension [31]	$\left[\frac{\sigma_2}{Y_T}\right]^2 + \left[\frac{\tau_{12}}{S_{12}}\right]^2 \leq 1$
Matrix Compression, Maximum Stress	$\left\|\frac{\sigma_2}{Y_C}\right\| \leq 1$
Matrix Compression [31]	$\left[\frac{\sigma_2}{Y_C}\right]^2 + \left[\frac{\tau_{12}}{S_{12}}\right]^2 \leq 1$
Fiber-Matrix Shear, Maximum Stress	$\left\|\frac{\tau_{12}}{S_{12}}\right\| \leq 1$
Fiber-Matrix Shear [30]	$\left[\frac{\sigma_1}{X_T}\right]^2 + \left[\frac{\tau_{12}}{S_{12}}\right]^2 \leq 1$
Delamination Initiation, Max Stress	$\left\|\frac{\sigma_3}{Z_T}\right\| \leq 1, \left\|\frac{\tau_{31}}{S_{31}}\right\| \leq 1, \left\|\frac{\tau_{23}}{S_{23}}\right\| \leq 1$
Delamination Initiation [30]	$\left[\frac{\sigma_3}{Z_T}\right]^2 + \left[\frac{\tau_{31}}{S_{31}}\right]^2 + \left[\frac{\tau_{23}}{S_{23}}\right]^2 \leq 1$

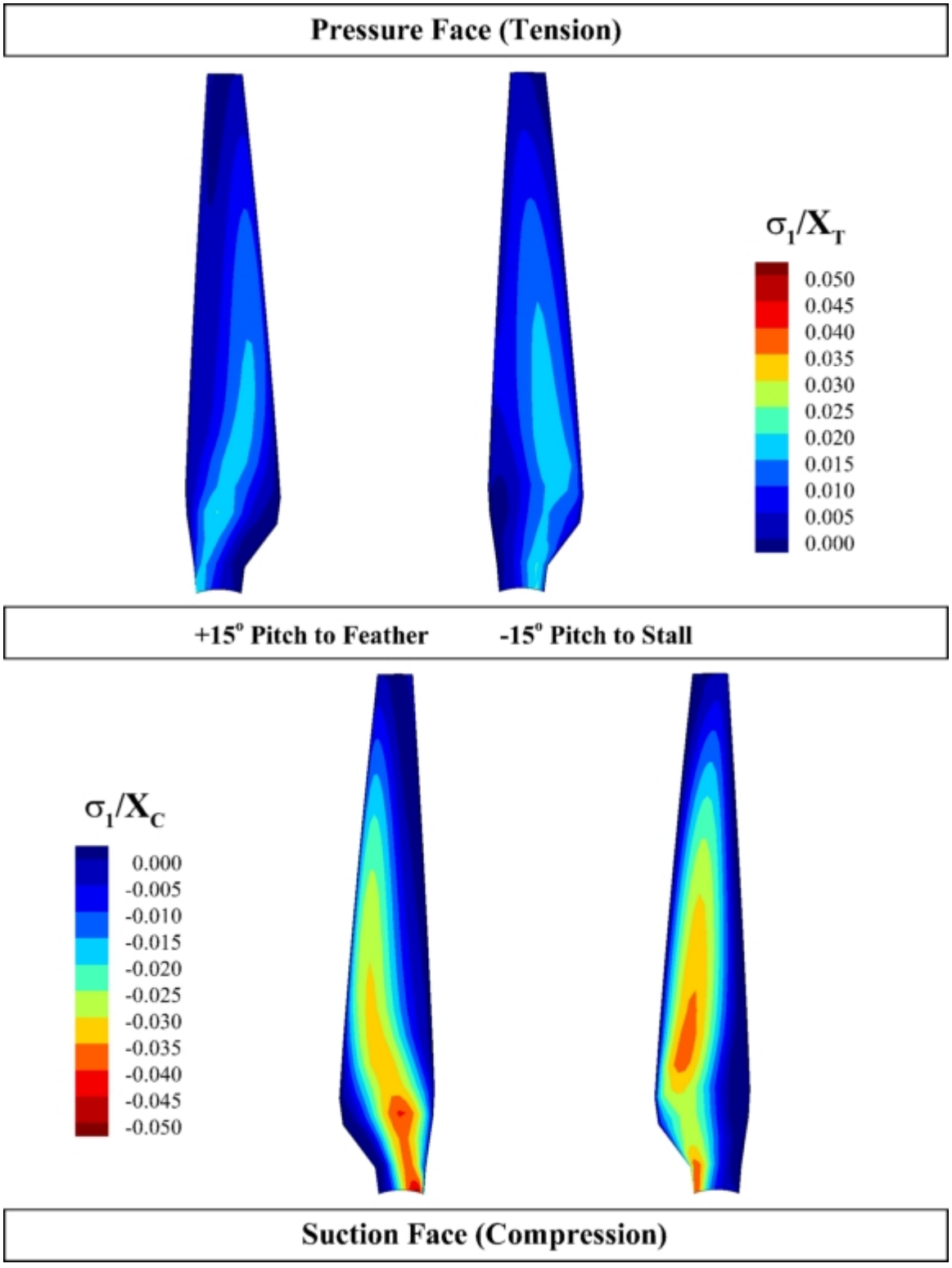

Figure 4.8: Fiber maximum stress failure indices in tension (top) and compression (bottom) for the $+15^\circ$ pitch to feather blade (left) and -15° pitch to stall blade (right).

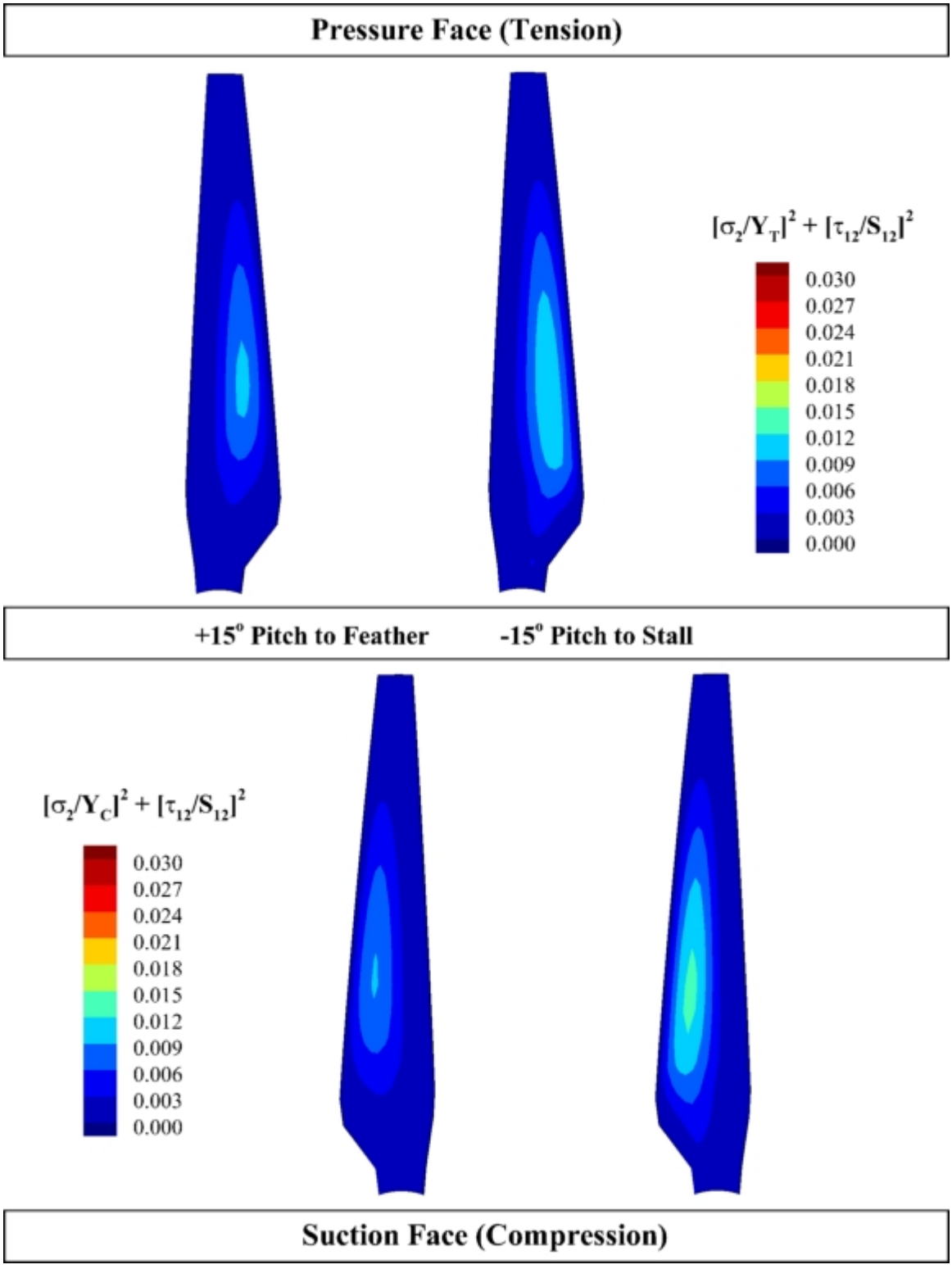

Figure 4.9: Hashin matrix failure indices in tension (top) and compression (bottom) for the $+15°$ pitch to feather blade (left) and $-15°$ pitch to stall blade (right).

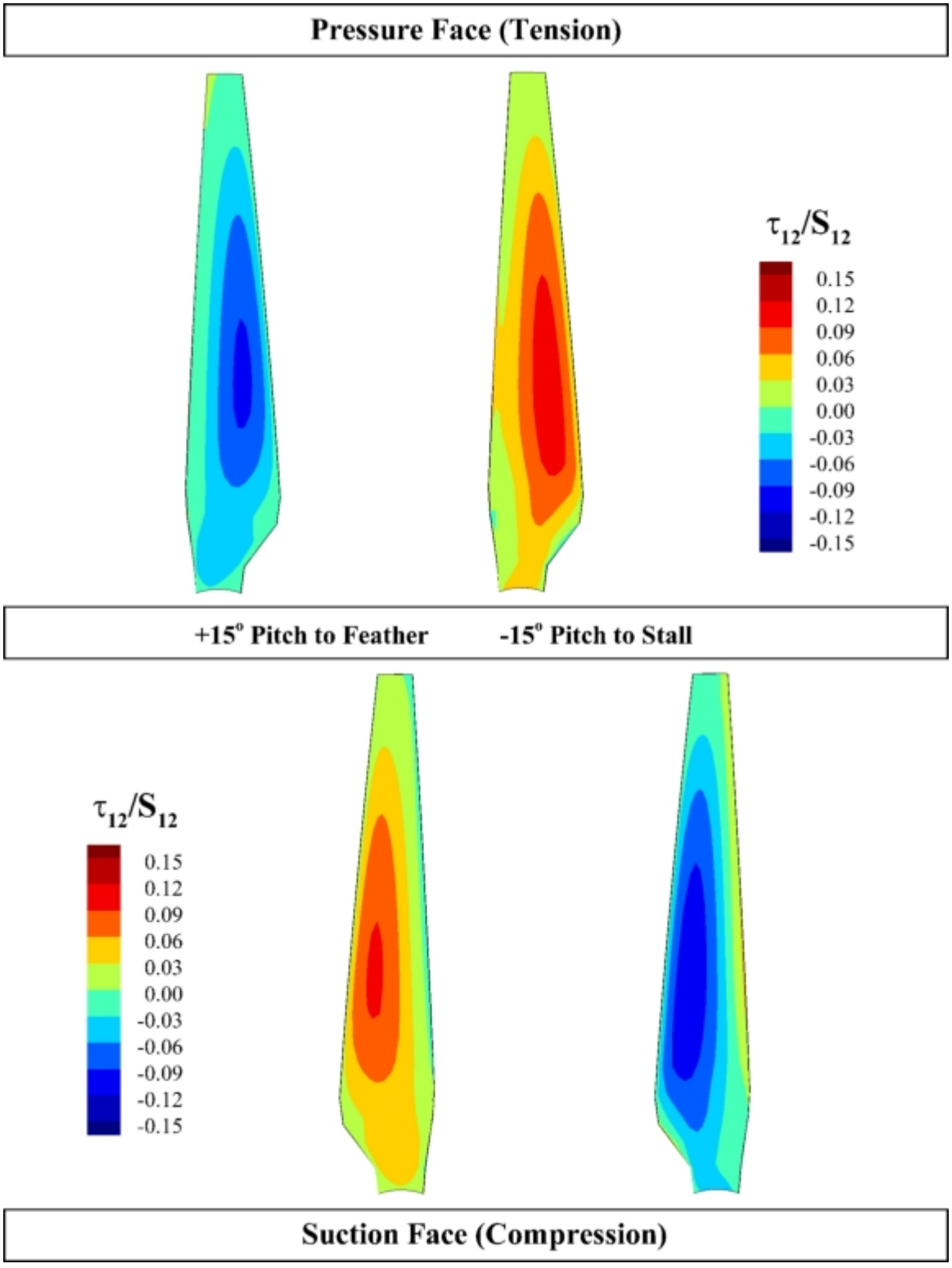

Figure 4.10: Fiber-matrix maximum shear stress failure indices for the +15° pitch to feather blade (left) and −15° pitch to stall blade (right).

the controlling failure mode of these blades. However, in general the failure indices of these blades are very low, suggesting that the system is significantly over-designed. In fact, while a solid blade model is useful to demonstrate the feasibility of tailoring the bend-twist properties of composite materials to create a passive pitch to feather or pitch to stall mechanism, it is not a practical representation of a commercial turbine blade. In Chapter 5, a more realistic design is considered and used to evaluate the lifetime performance and response of a passively adaptive turbine.

The structural analysis of the turbine blades shows that both passively controlled systems result in higher unsteady stress profiles than the reference blade model. This is due to the increased flexibility of the blades and the off-axis orientation of the fibers. The blade designed to pitch to stall, which produces higher power generation, displays higher stress concentrations than the pitch to feather blade. A general composite failure analysis showed a matrix-fiber maximum shear stress limit to be the controlling failure mode for both designs, followed by maximum tensile and compressive matrix and fiber failures, though the very low magnitude of the failure indices indicated that the solid blade models were overly robust under expected operating conditions.

Chapter 5

LIFETIME PERFORMANCE

To complete the results discussion, this chapter considers the likely long-term behavior of the adaptive turbine blades. First, a more advanced blade model is presented, and consequently that model used to examine the effects of fatigue-degraded strength and stiffness.

5.1 Advanced Blade Model

In order to more realistically predict stresses and asses the lifetime performance of a passively adaptive MHK turbine blade, it is necessary to create a more practical model. Tidal energy is still an emerging industry, and therefore has no standard or even widely accepted best section design method for the interior of the blade. However, a solid composite blade is not a very realistic approximation. MHK turbine blades are generally informed by those of the wind industry and feature a blade skin laid over structural spars or shear webs. This leaves the majority of the blade interior hollow, allowing for lighter-weight blades and lower material expense. Eventually, the model used in this work will need to be adapted to be able to contain empty cells and to more accurately represent the interior spars; for the scope of this study, only the first step towards that goal is taken. In this chapter, the blade model is evolved to represent a composite shell over a balsa wood core. The balsa wood acts as transverse shear reinforcement similar to the spars of a hollow blade and more accurately reflects the reduced weight and stiffness, but also provides the continuous structure needed in the current iteration of this model.

The balsa core blade is modeled with ten wrapping layers of even width stacked in the thickness direction. The outer two layers on the blade pressure and suction face are modeled as the same composite material as in the solid blade, while the inner layers use a lightweight balsa wood material model. Material properties of the balsa wood used for this model are shown in Table 5.1, and a schematic of the model layers is shown in Figure 5.1. The shell

thickness was chosen to be as thin as possible while maintaining the stability of the current model. Though this balsa core model is not a precise representation of an MHK turbine blade, it can still be an informative view into the response of a hollow spar blade. The lighter and less robust balsa core blades should trend in a similar fashion to a spar blade when compared to the solid model. This more realistic, balsa core model will allow greater accuracy in predicting lifetime behavior of the passively adaptive blades.

Table 5.1: Material Properties of Balsa Core.

$E = 3.76$ GPa
$G = 0.50$ GPa
$\nu = 0.05$

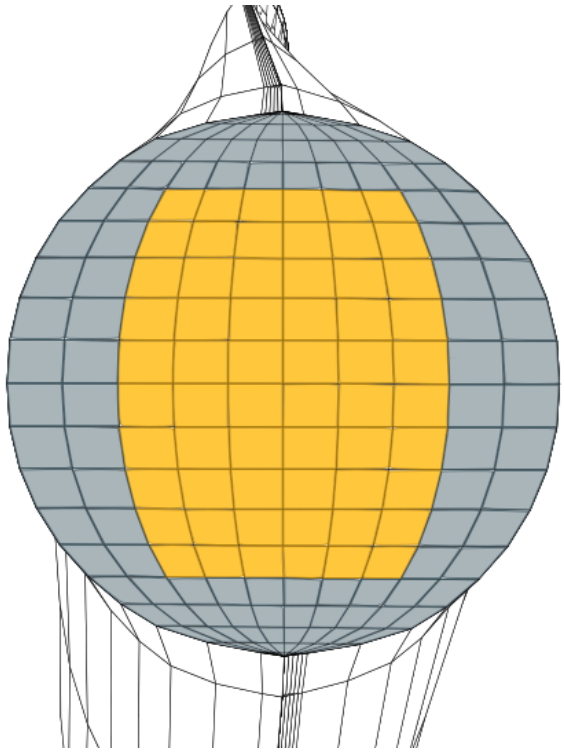

Figure 5.1: Material layers in the balsa core blades.

Before moving on to model the new blade, however, it is important to consider the lessons learned from the solid blade model. In order to improve computational efficiency, the thrust, stress, and loading trends shown in Chapters 3 and 4 are highly valuable. For each blade configuration, the peak reaction from and demand on the blade occurs at the point rated power is achieved, immediately before the initiation of active pitch mechanisms. Knowing this, the response of the balsa core blade need only be modeled for velocities ranging from cut-in speed to rated speed. This narrowing of the scope of the simulation provides a reduction in computational time of nearly 50%.

In that light, Figures 5.2-5.4 only show a velocity range up to the point of rated power for each blade. As anticipated, Figure 5.2 shows that the change in pitch of the balsa core blade is greater in magnitude than that of the solid blade. Intuitively, this should also extend the power, thrust and stress trends shown in Figs. 3.10, 3.11 and 4.2. The increased flexibility of the balsa core blades will cause larger changes in pitch, decreasing the angle of attack and power generation for the $+15°$ pitch to feather blade and increasing the angle of attack and power generation for the $-15°$ pitch to stall blade when compared to solid composite blades with the same material configuration.

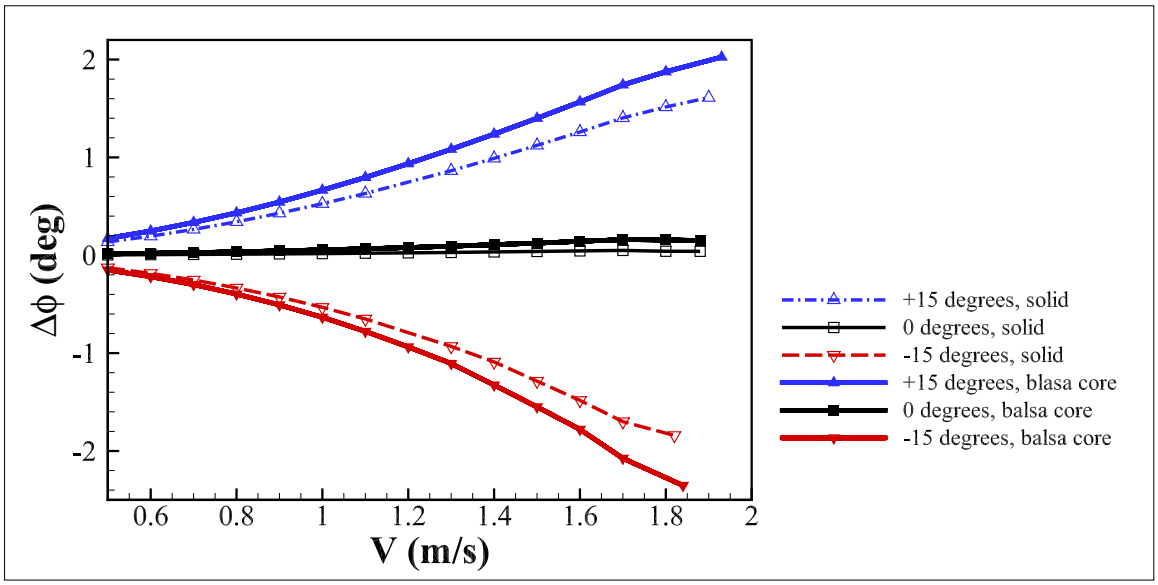

Figure 5.2: Change in pitch for the solid and balsa core blade models.

Figure 5.2 shows that the maximum change in pitch for each blade is not insignificant. However, Figures 5.3 and 5.4 show that though the change in power generation and total thrust trend as expected for the less robust blades, the magnitude of the change was found to be very small between the solid and balsa core blades. However, it is important to consider blade stresses as well. As demonstrated by Figs. 3.10 and 4.2 and discussed in Section 4.1, higher blade stresses do not necessarily correspond with greater power generation. Conversely, although the reduced blade section does not cause a large difference in power generation, the effects of higher flexibility have a significant impact on blade stresses.

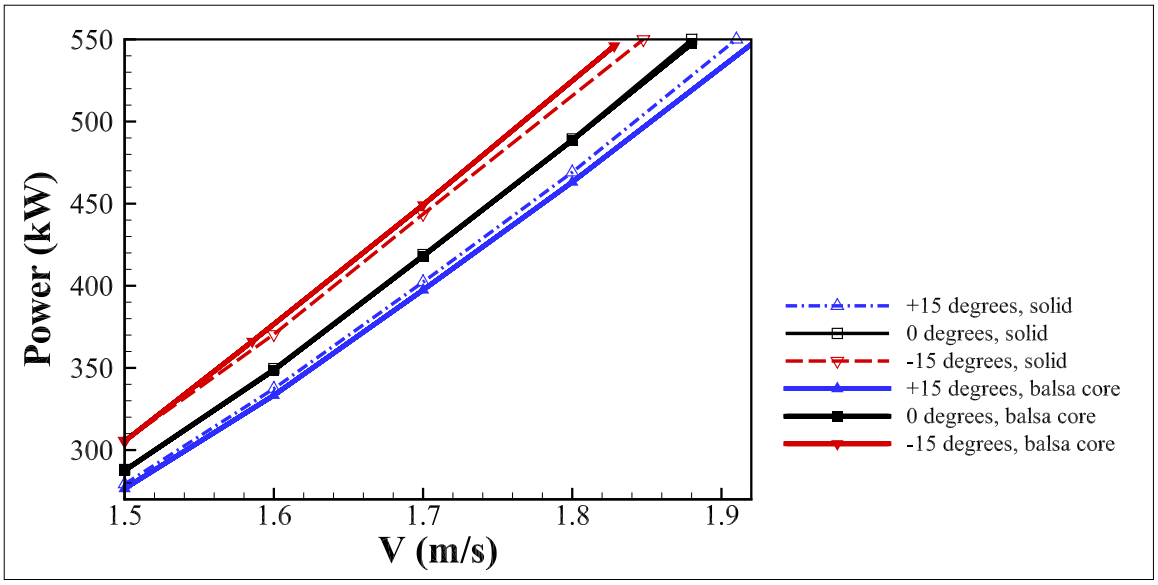

Figure 5.3: Predicted power generation for the solid and balsa core blade models.

Figures 5.5-5.7 show contours of the same composite failure indices as presented in Figures 4.8-4.10 in Section 4.2. As before, the tensile and compressive fiber maximum stress (shown in Figure 5.5), the matrix failure mechanism (Figure 5.6), and the fiber-matrix maximum shear stress (Figure 5.7) are the controlling failure modes. Figures 5.5-5.7 are plotted with the same contour limits as Figures 4.8-4.10 in Section 4.2, to facilitate comparisons of magnitude between the solid and balsa core blade models. For all three failure mechanisms, the stress concentrations and distribution shapes between the solid and

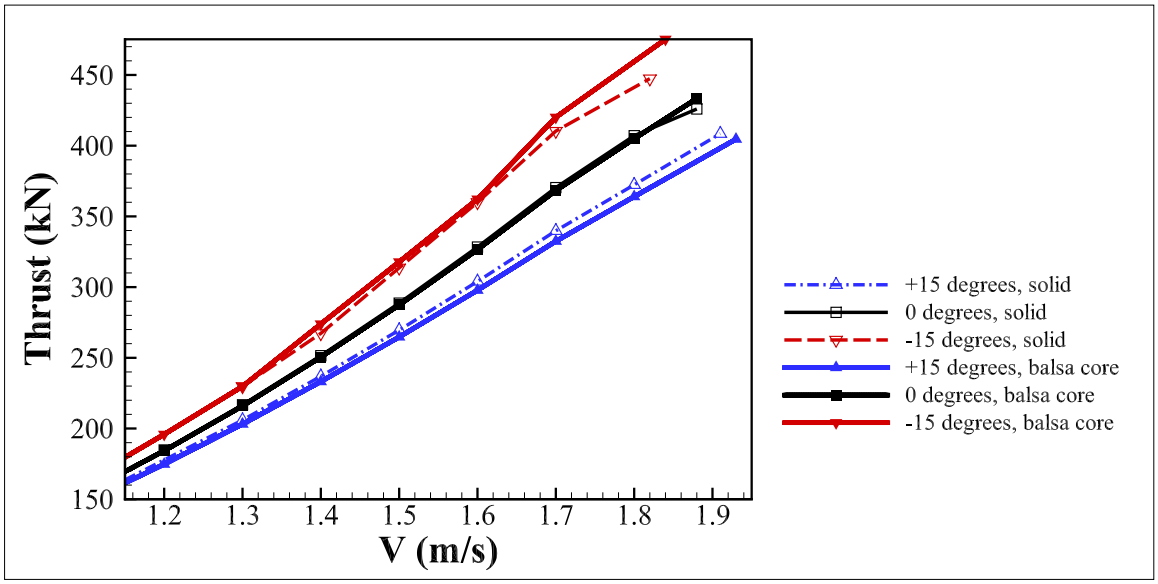

Figure 5.4: Predicted total thrust on the solid and balsa core blade models.

balsa core blades are the same. Each blade configuration, however, sees greater magnitude failure indications in the balsa core model than the solid model. Both of these observations align well with reasonable expectations for the more flexible blade.

5.2 Long Term Structural Response

The stress variations discussed above have critical implications for fatigue. This is true not just because of the chance of premature failure but also because higher stress amplitudes will correspond to larger decreases in bending strength and stiffness due to the accumulation of fatigue-induced damage. With the knowledge of composite fatigue degradation available presently, it is impossible to make an accurate prediction of the lifetime behavior of a bend-twist coupled turbine blade. It can be beneficial, however, to consider the general effects of strength and stiffness degradation and to examine the affect that these changes in the material properties could have on the performance of a system. While many fatigue analyses are designed to determine the ultimate fatigue life of a system, proper consideration of *stiffness* degradation effects in passively controlled structures is critical to determining sys-

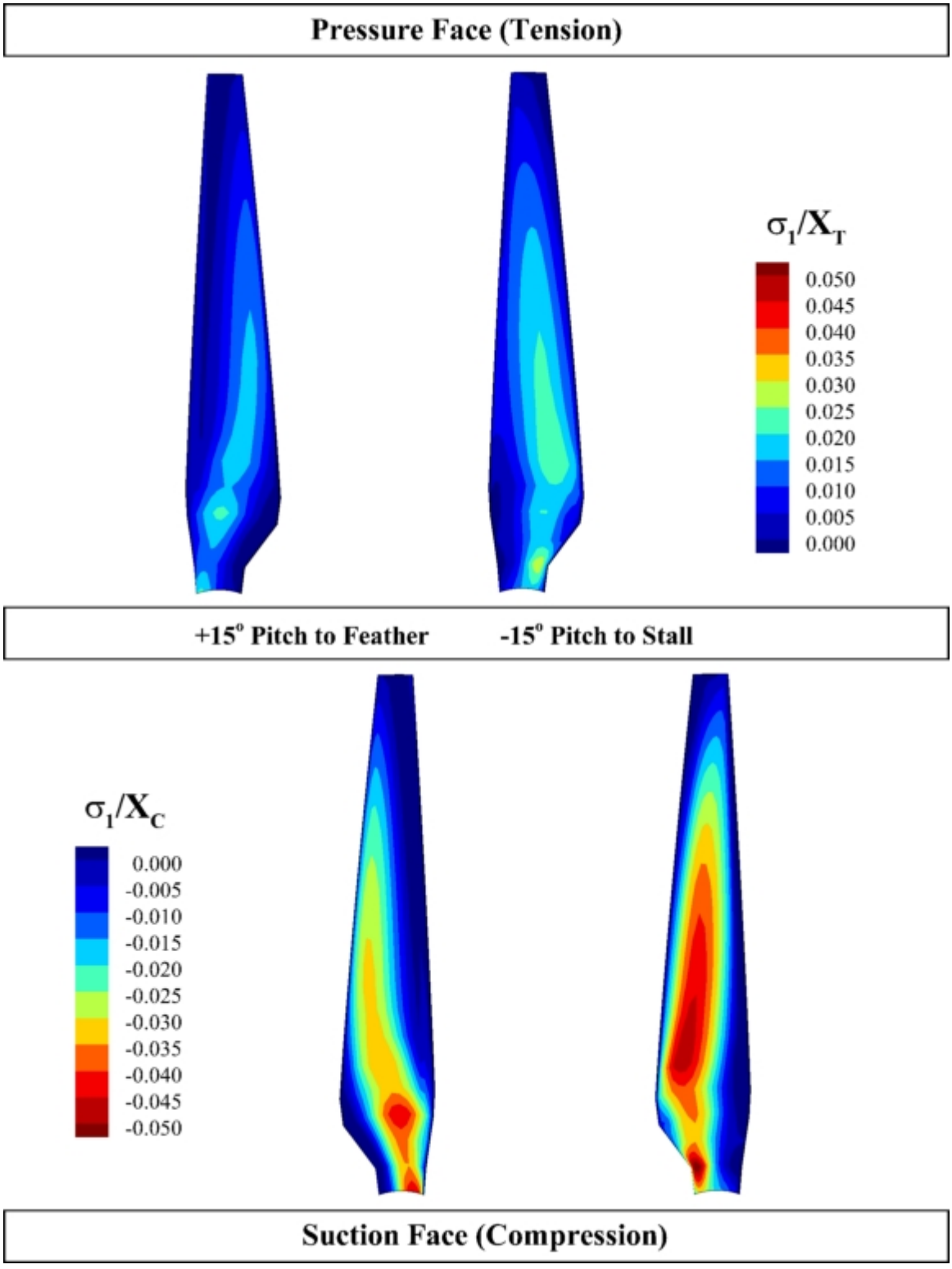

Figure 5.5: Fiber maximum stress failure indices in tension (top) and compression (bottom) for the $+15^\circ$ pitch to feather, blasa core blade (left) and -15° pitch to stall, balsa core blade blade (right).

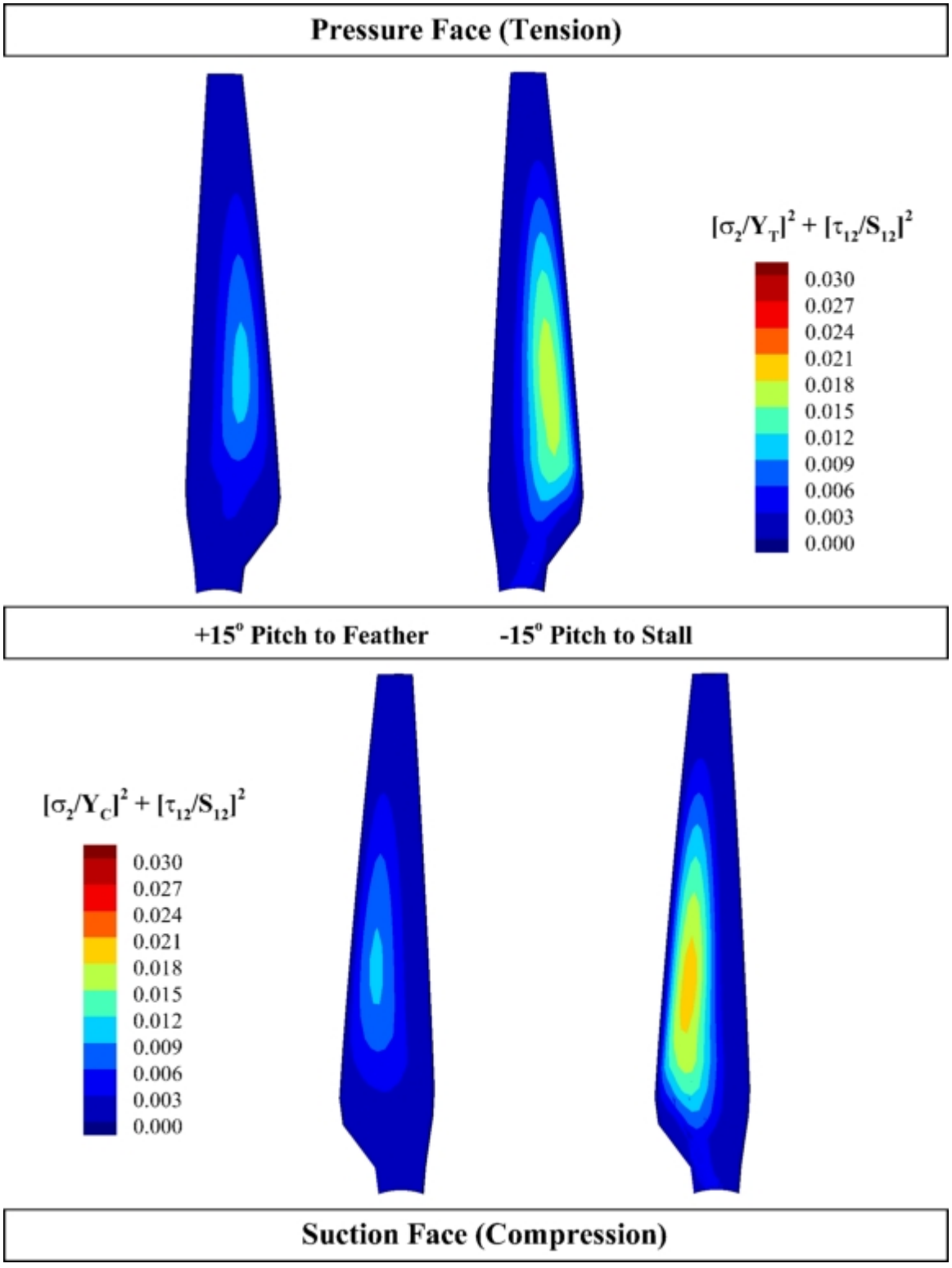

Figure 5.6: Hashin matrix failure indices in tension (top) and compression (bottom) for the $+15°$ pitch to feather, blasa core blade blade (left) and $-15°$ pitch to stall, balsa core blade blade (right).

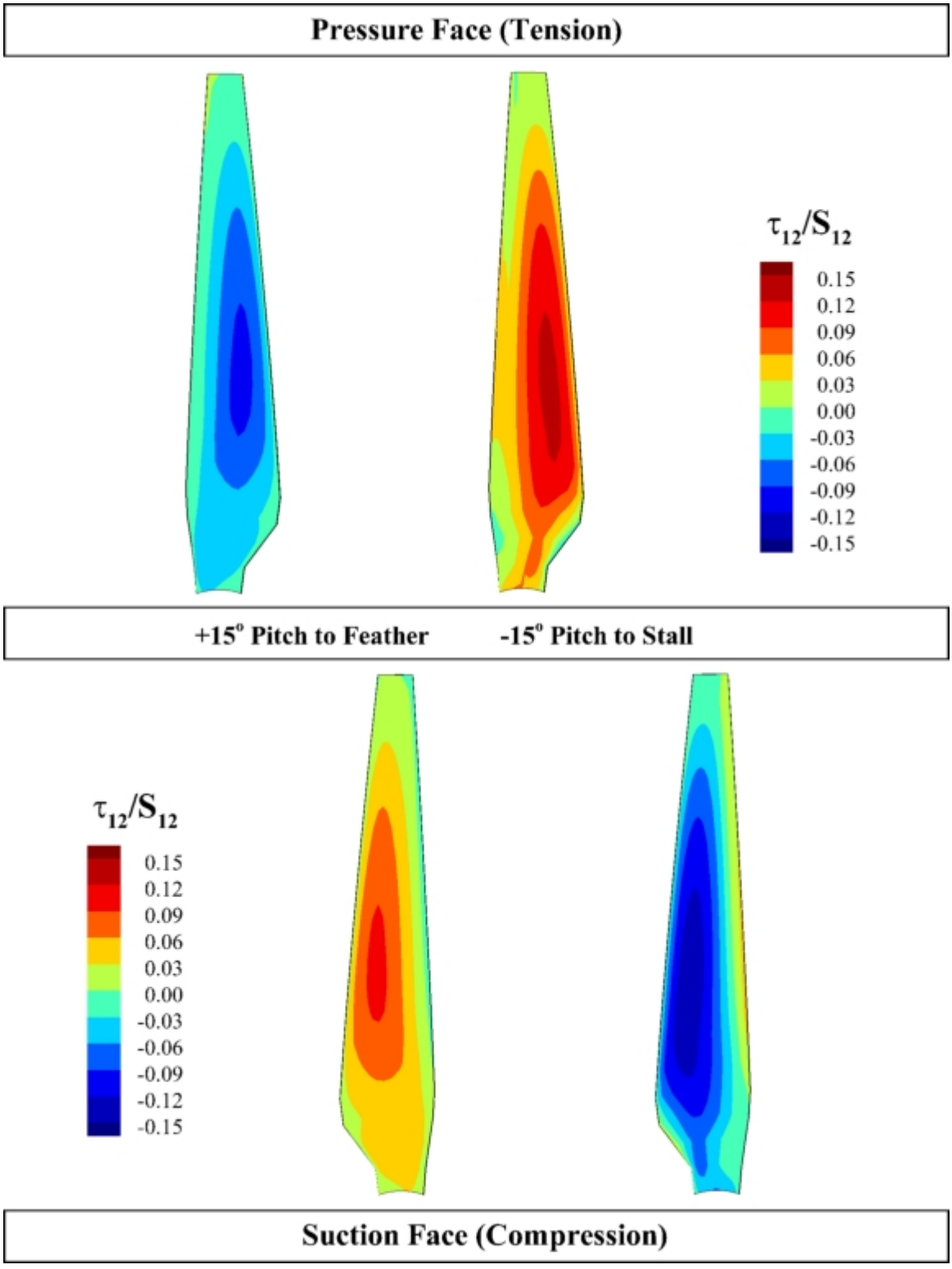

Figure 5.7: Fiber-matrix maximum shear stress failure indices for the +15° pitch to feather, blasa core blade blade (left) and −15° pitch to stall blade, balsa core blade (right).

tem performance under long-term variable amplitude loading. This is essential because the performance of the system is largely dependent on the deformed geometry of the structure, which in turn is a function of the material stiffness.

For an adaptive pitch MHK turbine, the performance of the system relies on the load-dependent deformation response of the blades. As this in turn depends on the bending stiffness, predicting the long-term performance requires a fundamental knowledge of the fatigue behavior of the material. In addition to a detailed description of the load spectrum and history, fatigue analysis requires a thorough understanding of the long-term behavior of the material. The anisotropic nature of a composite turbine blade can be difficult to quantify, and inherent flaws such as microcracks, misalignments, and voids in the material can be expected. While it is well understood that the strength and stiffness of composite materials degrade over time, the rate and extent of degradation can fluctuate significantly due to loading sequence, material imperfections, and the effects of salt water or temperature. Further, significant experimental testing is required to determine a method for quantifying material degradation in terms of the constitutive material model essential for a numerical analysis of the long term effects of variable amplitude loading. Attempts to estimate a precise fatigue life of a composite structure can be impractical when considering the extent of modeling, loading, and material uncertainties that exist at this time.

However, it is useful to model the qualitative effect of a reduction in strength and stiffness. To that effect, Figure 5.8 shows the predicted change in blade pitch of the balsa core blades for the reference model and two adaptive blades, with and without consideration for degradation effects. When the blade stiffnesses (bending and shear modulii) are reduced by 10% and the tensile, compressive and shear strengths reduced by 20%, the passively controlled blades tend to become more flexible and resulting deformations increase.

This increase in flexibility due to fatigue will further extend the trends noted for the comparison between the solid and balsa core blade models above. The passive pitch adjustment of a $+15^\circ$ pitch to feather blade will increase over time, decreasing the angle of attack and power generation of the blade, and a -15° pitch to stall blade will do the opposite. Again, though the change in pitch is non-negligible, it is smaller in proportion to the change found between the solid and balsa core blades, and the effect to power production

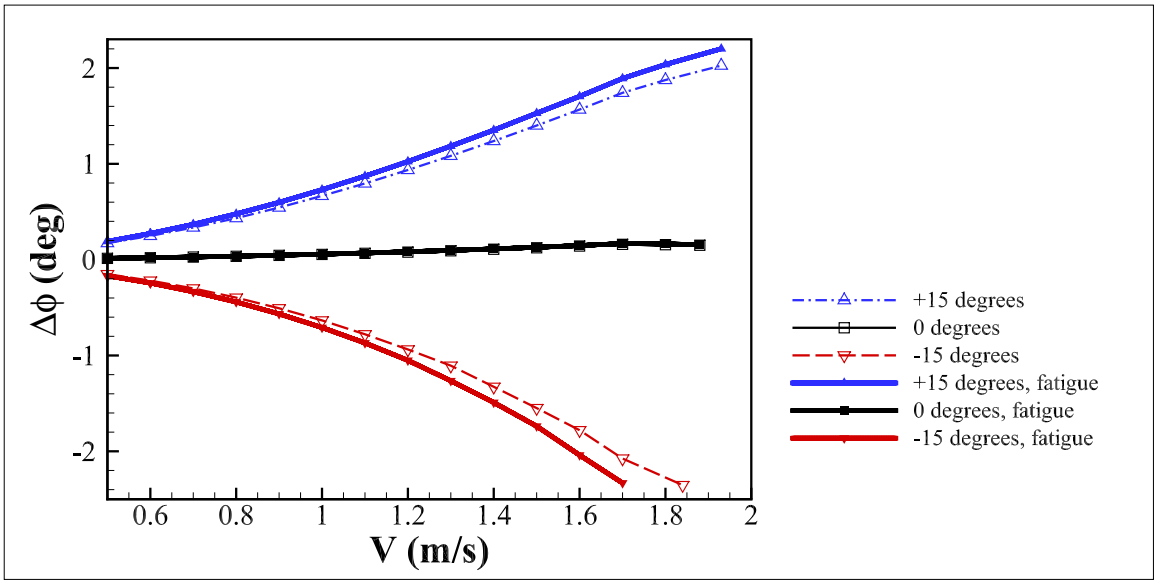

Figure 5.8: Change in pitch for the balsa core blade models under degraded strength and stiffness conditions.

and system thrust produced by such a difference in pitch change was shown to be essentially insignificant to the accuracy of this model. It can therefore be concluded that at this stage of stiffness degradation, turbine performance is not strongly impacted by fatigue of the blades.

Though preliminary considerations of fatigue do not appear to greatly affect the power generation of the system, long term strength and stiffness degradation must be carefully considered due to the likely increase in blade stresses and, consequently, failure indices. The increased flexibility causes greater stresses, which are placed in the numerator of the failure index. That coupled with the decrease in strength, reflected in the denominator of the index, expedite potential failure initiation. As seen above, a small increase in flexibility can create a strong effect on the structural response of the blade. Likewise, the consequence of strength and stiffness degradation have a significant impact on blade stresses. Figures 5.9-5.11 demonstrate the impact of that degradation on the pitch to feather and pitch to stall balsa core blade models. Again, the plots are shown with contour limits consistent with

those in previous failure index figures. Unsurprisingly, there is no change in the general trend of stress distributions, while the magnitude of the failure indices have increased. Table 5.2 compares the change in pitch and the maximum failure index for each of the three controlling modes for the solid, balsa core, and strength and stiffness degraded balsa core blade models at $V = 1.7$ m/s. From this table two correlations between the blade flexibility and the failure index are clear. Higher flexibility results in higher failure indices, and pitch to feather blades show lower indications of failure than corresponding pitch to stall models. It is also worth noting that none of the controlling modes approach a failure index of unity. Even in the circumstance that a large safety factor is applied to account for the many uncertainties inherent to the material and to systems operating in the harsh offshore marine environment, the blades are potentially overly robust. This will be explored in future work with a more realistic, hollow spar blade model.

Table 5.2: Change in pitch and maximum magnitude failure indices in controlling modes for various blade models at $V = 1.7$ m/s.

	Solid Blade		Balsa Core Blade		Fatigued Blade	
Parameter	$+15°$	$-15°$	$+15°$	$-15°$	$+15°$	$-15°$
$\Delta\phi$	1.404	-1.700	1.741	-2.075	1.891	-2.330
Fiber Failure	0.044	0.058	0.048	0.087	0.057	0.110
Matrix Failure	0.010	0.013	0.012	0.020	0.018	0.032
Shear Failure	0.098	0.112	0.100	0.140	0.124	0.176

In this chapter, more advanced blade models are examined to better represent realistic blade sections. The less robust, balsa core blade models are shown to behave in a more flexible manner than the preliminary solid models, magnifying the stress and performance trends found for the solid blades. Though a thorough fatigue analysis is infeasible with the current available knowledge, strength and stiffness degradation is modeled to provide an estimate for lifetime performance. Over time, the reduced stiffness of the blades will

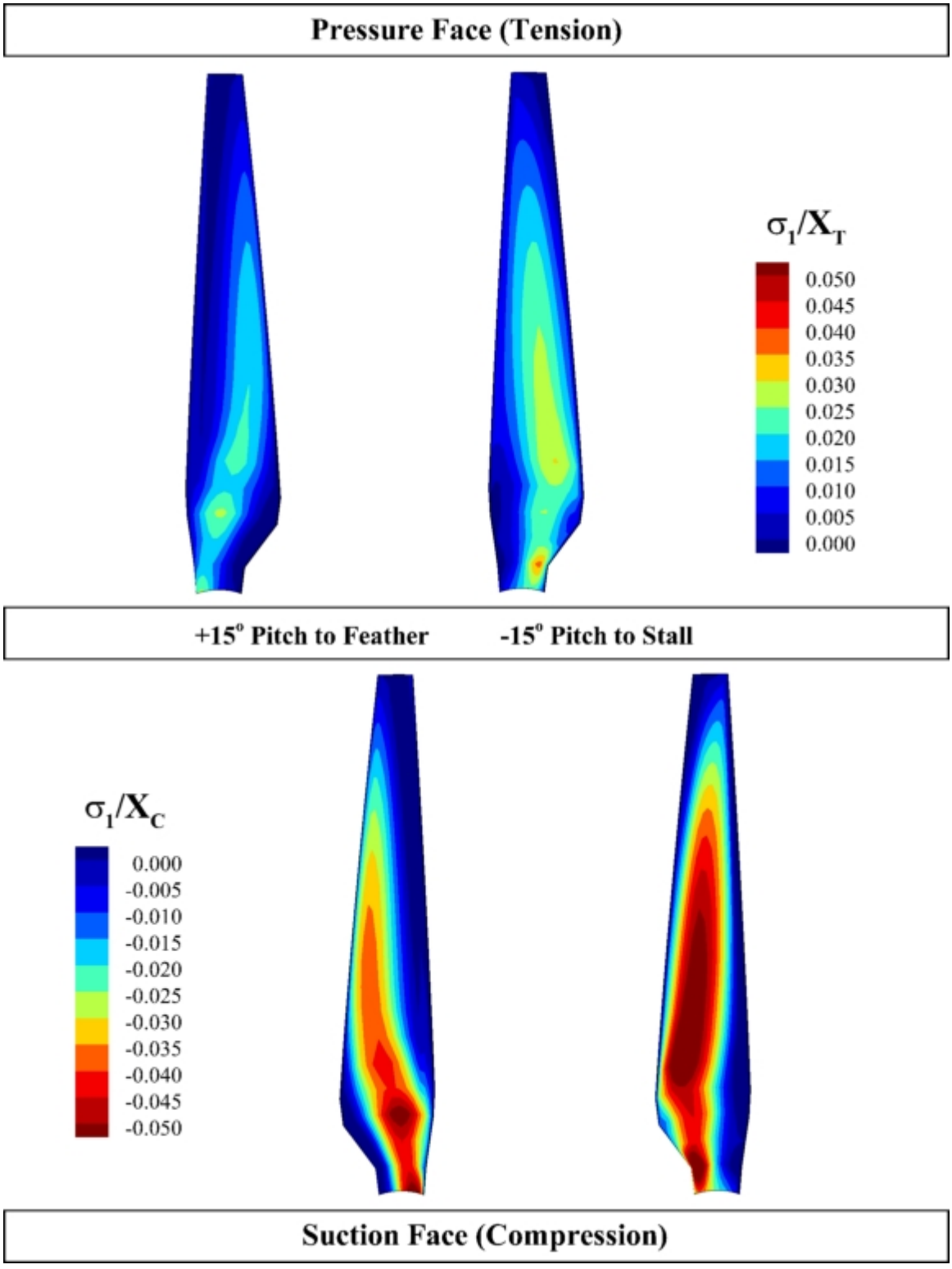

Figure 5.9: Fiber maximum stress failure indices in tension (top) and compression (bottom) for the $+15^\circ$ pitch to feather blade (left) and -15° pitch to stall blade (right) under degraded strength and stiffness conditions.

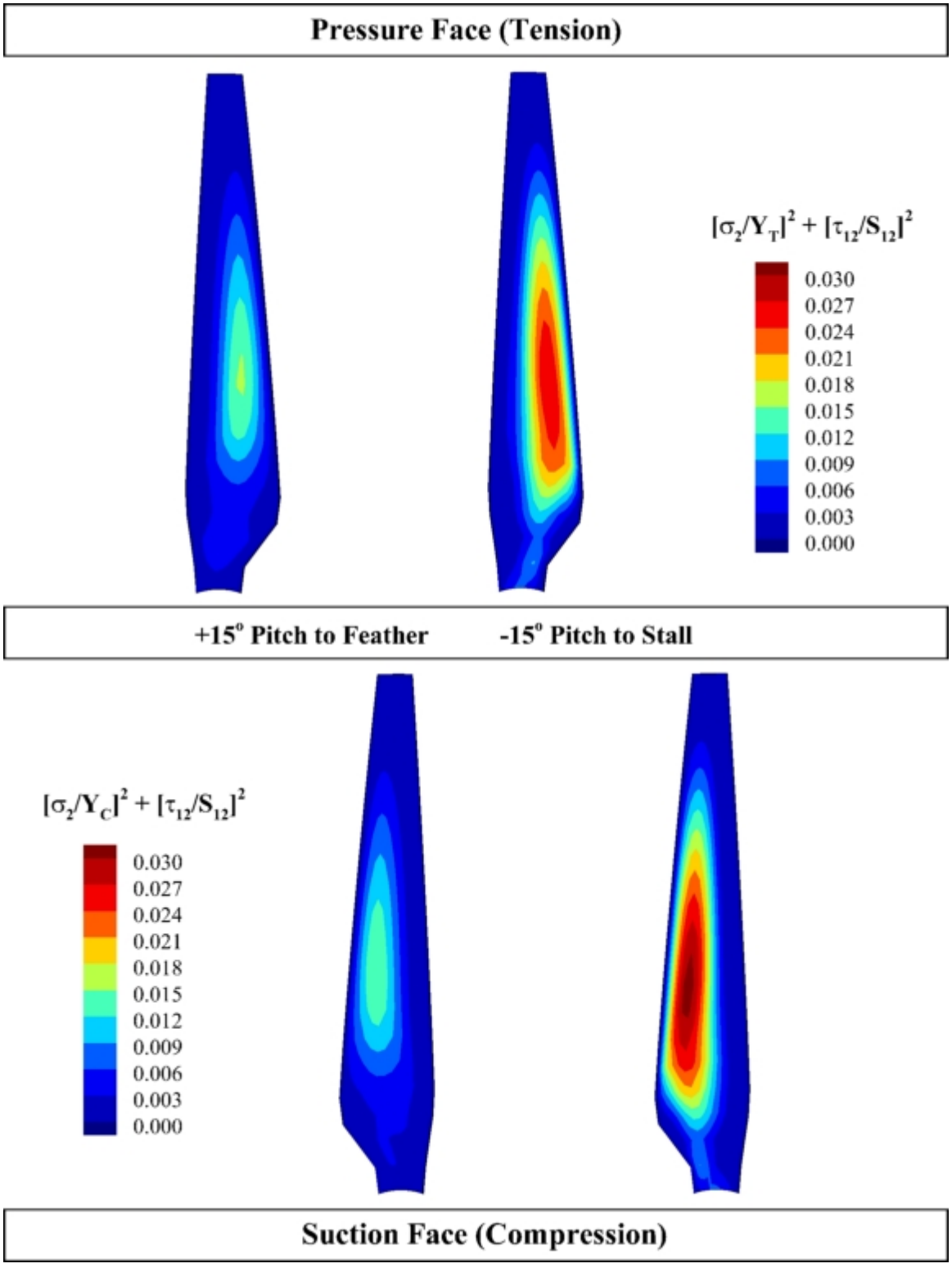

Figure 5.10: Hashin matrix failure indices in tension (top) and compression (bottom) for the $+15°$ pitch to feather blade (left) and $-15°$ pitch to stall blade (right) under degraded strength and stiffness conditions.

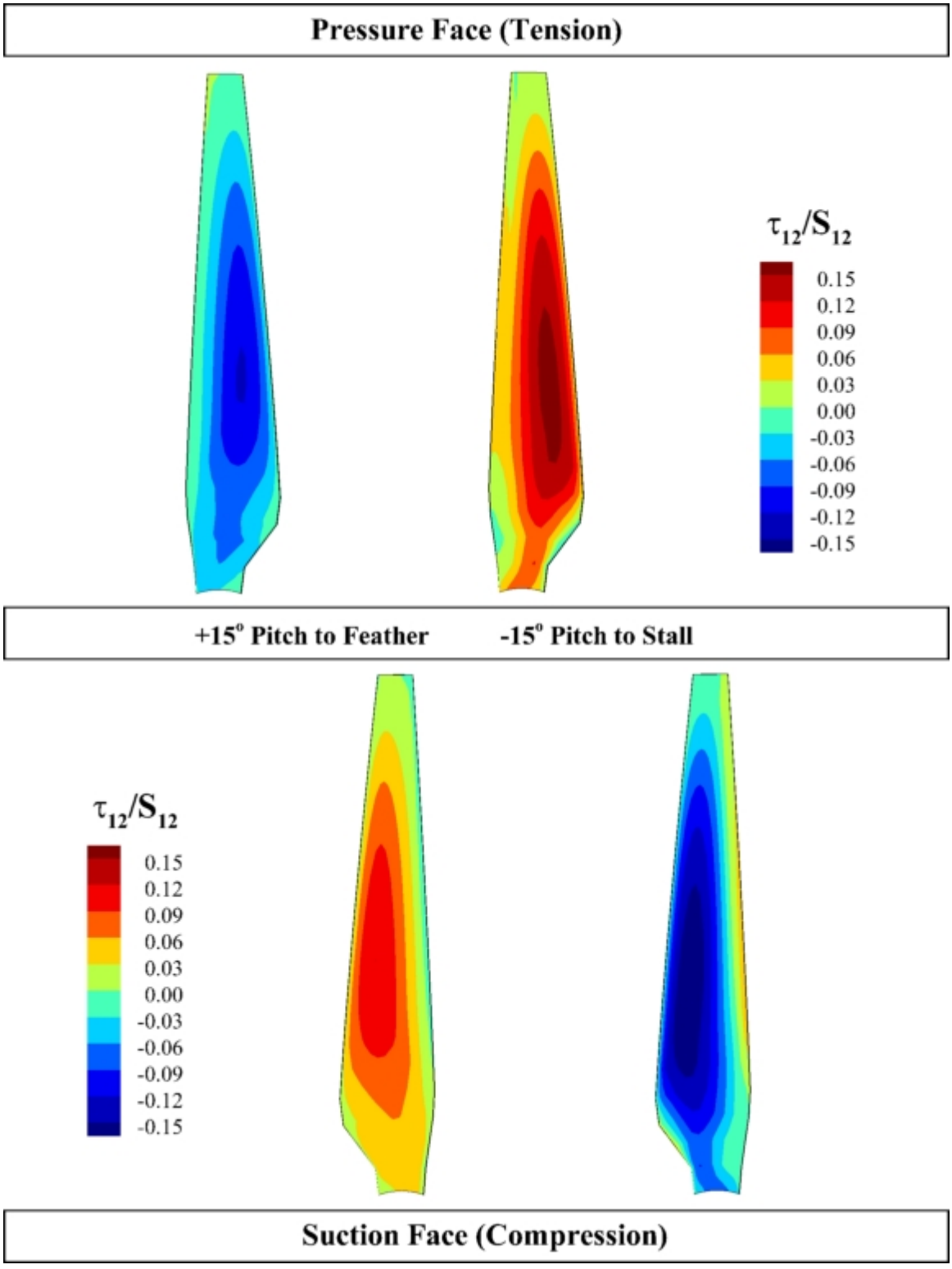

Figure 5.11: Fiber-matrix maximum shear stress failure indices for the $+15°$ pitch to feather blade (left) and $-15°$ pitch to stall blade (right) under degraded strength and stiffness conditions.

result in greater flexibility and thus increased passive deformations. The failure analyses for the degraded blades suggest that the structural demand on the system is not unreasonable; however, a more realistic blade model and a better understanding of the impact of fatigue on the coupled bend-twist material behavior is needed to verify that conclusion.

Chapter 6

CONCLUSIONS AND FUTURE WORK

6.1 Conclusions

This work examines the capabilities of passive pitch control of marine hydrokinetic (MHK) turbine blades under both instantaneous and long-term variable amplitude loading with consideration for practical design and operational constraints. Because most MHK turbine blades are constructed from composite materials, hydroelastic tailoring of the material can provide improved performance over the expected operational life of the system through development of a rapid, passive bend-twist coupling mechanism. Potential performance improvements include increased power generation, reduced hydrodynamic instabilities, and improvements in efficiency, load shedding, and structural performance. A summary of the conclusions drawn in presented in Table 6.1 and outlined in more detail below.

Table 6.1: Summary of Conclusions

Parameter	Pitch to Feather Blades ($\theta_{eq} > 0$)	Pitch to Stall Blades ($\theta_{eq} < 0$)
Blade Pitch (ϕ)	Increased	Decreased
Angle of Attack (α)	Decreased	Increased
Power Output	Decreased	Increased
Blade Loads	Decreased	Increased
Active Pitch Requirements	Decreased	Increased

Preliminary studies on a solid composite blade model show that the orientation of the composite fibers can be tailored to create turbine blades that pitch to stall or pitch to feather, depending on the direction of an equivalent unidirectional fiber angle from the radial line

of the blade. Passively controlled blades that pitch to feather are shown to decrease angle of attack and therefore energy capture when compared to a reference blade with no passive pitch mechanism, while blades designed to pitch to stall increase angle of attack and energy capture.

Practical restrictions imposed on turbine systems such as maximum rotational speed or generated power are shown to create tradeoffs and limits on these performance improvements. Thus, fair comparisons between systems must rely on the local flow environment to properly address dimensional blade loads. Those blades that increase power production were also shown to experience higher blade loads and increase the required range for active control, while those blades that decrease power production were shown to result in lower blade loads and decreased active control requirements. Neither system displayed enough of a shift in active pitch requirements to suggest that a passive control mechanism could entirely replace active control, but a blade could be designed to reduce the amount of time an active control mechanism would be required. Such a blade would, however, have a decreased rate of energy production.

From the structural analysis of the turbine blades, both passively controlled systems resulted in higher unsteady stress profiles than the reference blade model. This was due to the increased flexibility of the blades and the off-axis orientation of the fibers. The blade designed to pitch to stall, which produced higher power generation, displayed higher stress concentrations than the pitch to feather blade. A general composite failure analysis showed a matrix-fiber maximum shear stress limit to be the controlling failure mode for both designs, followed by maximum tensile and compressive matrix and fiber failures, though the very low magnitude of the failure indices indicated that the solid blade models were overly robust under expected operating conditions.

More advanced blade models were examined to better represent realistic blade sections. The less robust, balsa core blade models are shown to behave in a more flexible manner than the preliminary solid models, magnifying the stress and performance trends found for the solid blades. Though a thorough fatigue analysis is concluded to be infeasible with the current available knowledge, strength and stiffness degradation is modeled to provide an estimate for lifetime performance. Over time, the reduced stiffness of the blades was

shown to result in greater flexibility and thus increased passive deformations; care must therefore be taken to ensure that the turbine will operate within the practical constraints of the system over its expected operational life. The failure analyses for the degraded blades suggest that the structural demand on the system is not unreasonable; however, a more realistic blade model and a better understanding of the impact of fatigue on the coupled bend-twist material behavior is needed to verify that conclusion.

6.2 Future Work

The results presented here indicate that passive pitch control of MHK turbine blades has the potential to improve overall system performance. The performance improvements shown are based only on modifying the material properties of the DOE Reference Model turbine, and thus a critical next step in this research is to create a more detailed blade model that can more accurately represent the structural spars and hollow interior featured in most typical wind and marine turbine blades. This can be expected to create a more flexible blade and allow for a more precise prediction of blade stresses. The model can then be used to optimize the blade design with considerations for both geometric and material parameters in an attempt to reduce the tradeoffs in performance shown in this work.

The blades in this study do not experience fluid cavitation; however, passive control has been shown to reduce the susceptibility for cavitation in propellers. This is currently being explored for turbine systems as well, creating the possibility of higher maximum rotational speeds, less active control, and higher energy capture. With more precise blade models cavitation will need to be examined and the limiting parameters explored in more depth.

In order to predict the lifetime response of a turbine, the development of an experimental program for the consideration of long-term fatigue effects is also essential. There is currently very little known about the effects of fatigue on the bend-twist mechanism of composite materials, especially such materials operating in the submarine environment. This makes lifetime performance impossible to quantify, as the passive pitch control mechanism, which defines system performance, relies on this load-dependent deformation response of the blades. An extensive study into fatigue behavior is needed to inform material constitutive models and failure mechanism limits for a more accurate structural model of the turbine

blades.

Lastly, an examination of the BEM solver used in this work is recommended. In the adaptation of the code from propellers to turbines, no account was made for the axial or angular induction factors which represent the slowing and rotation of the fluid in the free stream due to the blockage and wake created by the turbine rotor. This error is causing the predicted power coefficients to be higher than realistic, in cases approaching or even reaching the theoretical Betz limit, which defines the maximum possible power coefficient for an ideal turbine system. This should not greatly affect the present work due to the fact that the conclusions made here are relative in nature between different blade models, but should be corrected for a more accurate estimation of the possible power output of a given turbine system.

BIBLIOGRAPHY

[1] ABAQUS. *ABAQUS Version 12.3 Documentation*. ABAQUS, Inc., 2012.

[2] Advanced Composites Manufacturing Centre. Composite design and manufacture. http://www.tech.plym.ac.uk/sme/MATS324/MATS324A4%20fracture.htm, 2014.

[3] T.D. Ashwill. Passive load control for large wind turbines. In *51st AIAA/ASME/ASCE/AHS/ASC Structures, Structural Dynamics, and Materials Conference*, April 2010.

[4] A.S. Bahaj, W.M.J. Batten, and G. McCann. Experimental verifications of numerical predictions for the hydrodynamic performance of horizontal axis marine current turbines. *Renewable Energy*, 32:2479–2490, 2007.

[5] A.S. Bahaj and L.E. Myers. Fundamentals applicable to the utilisation of marine current turbines for energy production. *Renewable Energy*, 28:2205–2211, 2003.

[6] N. Barltrop, K.S. Varyant, A. Grant, D. Clelland, and X. Pham. Wave-current interactions in marine current turbines. In *Proceedings of the Institution of Mechanical Engineers, Part M: Journal of Engineering for the Maritime Environment*, 2006.

[7] W.M.J. Batten, A.S. Bahaj, A.F. Molland, and J.R. Chaplin. Hydrodynamics of marine current turbines. *Renewable Energy*, 31:249–256, 2006.

[8] W.M.J. Batten, A.S. Bahaj, A.F. Molland, and J.R. Chaplin. Experimentally validated numerical method for the hydrodynamic design of horizontal axis tidal turbines. *Ocean Engineering*, 34:1013–1020, 2007.

[9] W.M.J. Batten, A.S. Bahaj, A.F. Molland, and J.R. Chaplin. The prediction of the hydrodynamic performance of marine current turbines. *Renewable Energy*, 33:1085–1096, 2008.

[10] S.E. Ben Elghali, M.E.H. Benbouzid, and J.F. Charpentier. Marine tidal current electric power generation technology: state of the art and current status. In *Electric Machines & Drives Conference*, 2007.

[11] A. Beyene and J. Peffley. Constructual theory, adaptive motion, and their theoretical application to low-speed turbine design. *Journal of Energy Engineering*, pages 112–118, December 2009.

[12] G.S. Bir, M.J. Lawson, and Y. Li. Structural design of a horizontal-axis tidal current turbine composite blade. In *International Conference on Ocean, Offshore and Arctic Engineering*, June 2011.

[13] L.S. Blunden and A.S. Bahaj. Tidal energy resource assessment for tidal stream generators. *Journal of Power and Energy*, 221(2):137–146, 2007.

[14] I. Bryden and G.T. Melville. Choosing and evaluating sites for tidal current development. *Journal of Power and Energy*, 218, 2004.

[15] I.G. Bryden and S.J. Couch. Me1 - marine energy extraction: tidal resource analysis. *Renewable Energy*, 31:133–139, 2006.

[16] P. Camanho and M. Lambert. A design methodology for mechanically fastened joints in laminated composite materials. *Composites Science and Technology*, 66:3004–3020, 2006.

[17] B. Chen, S. Neely, T. Michael, S. Gowing, R. Szwerc, D. Buchler, and R. Schult. Design, fabrication and testing of pitch-adapting (flexible) composite propellers. In *The SNAME Propellers/Shafting Symposium '06*, Virginia Beach, VA, 2006.

[18] P. Davies, G. Germain, B. Gaurier, A. Boisseau, and D. Perreux. Evaluation of the durability of composite tidal turbine blades. *Philosophical Transactions of the Royal Society A*, 371(1985), 2013.

[19] W.C. de Goeij, M.J.L. van Tooren, and A. Beukers. Implementation of bending-torsion coupling in the design of a wind-turbine rotor-blade. *Applied Energy*, 63:191–207, 1999.

[20] P.L. Fraenkel. Power from marine currents. *Journal of Power and Energy*, 216, 2002.

[21] P.L. Fraenkel. Marine current turbines: Pioneering the development of marine kinetic energy converters. In *Proceedings of the Institution of Mechanical Engineers, Part A: Journal of Power and Energy*, volume 221, pages 159–169, 2007.

[22] P.P. Friedmann, C. Venkatesan, and K. Yuan. Development of a structural optimization capability for the aeroelastic tailoring of composite rotor blades with straight and swept tips. In *4th AIAA Symposium on Multidisciplinary Analysis and Optimization*, Cleveland, OH, 1992.

[23] R. Ganguli and I. Chopra. Aeroelastic optimization of a composite helicopter rotor. In *4th AIAA Symposium on Multidisciplinary Analysis and Optimization*, Cleveland, OH, 1992.

[24] R. Ganguli and I. Chopra. Aeroelastic tailoring of composite couplings and blade geometry of a helicopter rotor using optimization methods. *Journal of American Helicopter Society*, 42(3):218–228, 1997.

[25] V.J. Ginter and J.K. Pieper. Robust gain scheduled control of a hydrokinetic turbine. *IEEE Transactions on Control Systems Technology*, 19(4), July 2011.

[26] B. Glaz, P. Friedmann, and L. Lu. Helicopter vibration reduction throughout the entire flight envelope using surrogate-based optimization. *Journal of American Helicopter Society*, 54(1):012007, 2009.

[27] S. Gowing, P. Coffin, and C. Dai. Hydrofoil cavitation improvements with elastically coupled composite materials. In *Proceeding of 25th American Towing Tank Conference*, Iowa City, IA, 1998.

[28] D. Griffin. Evaluation of design concepts for adaptive wind turbines, sand report 2002-2424. Technical report, Sandia National Laboratories, USA, 2002.

[29] D.M. Grogan, S.B. Leen, C.R. Kennedy, and C.M. Ó Brádaigh. Design of composite tidal turbine blades. *Renewable Energy*, 57:151–162, 2013.

[30] Z. Hashin. Failure criteria for unidirectional fiber composites. *Journal of Applied Mechanics*, 47(2):329–334, 1980.

[31] Z. Hashin and A. Rotem. A fatigue failure criterion for fiber reinforced materials. *Journal of Composite Materials*, 7(4):448–464, 1973.

[32] N.M. Karaolis, P.J. Mussgrove, and G. Jeronimidis. Active and passive aeroelastic power control using asymmetric fibre reinforced laminates for wind turbine blades. In *10th British Wind Energy Conference*, London, 1988.

[33] B.S. Kim, S.Y Bae, W.J. Kim, S.L. Lee, and M.K. Kim. A study on the design assessment of a 50kw ocean current turbine using fluid structure interaction analysis. In *26th IAHR Symposium on Hydraulic Machinery and Systems*, 2012.

[34] S.A. Kinnas and N.E. Fine. A numerical nonlinear analysis of the flow around two- and three-dimensional partially cavitating hydrofoils. *Journal of Fluid Mechanics*, 254:151–181, 1993.

[35] P. Kumar and R.P. Saini. Study of cavitation in hydro turbines - a review. *Renewable and Sustainable Energy Reviews*, 14:374–383, 2010.

[36] M.J. Lawson, Y. Li, and D.C. Sale. Development and verification of a computational fluid dynamics model of a horizontal-axis tidal current turbine. In *30th International Conference on Ocean, Offshore, and Arctic Engineering*, June 2011.

[37] A.T. Lee and R.G.J. Flay. Compliant blades for passive power control of wind turbines. *Wind Engineering*, 24:3–11, 2000.

[38] Y.J. Lee and C.C. Lin. Optimized design of composite propeller. *Mechanics of Advanced Materials and Structures*, 11:17–30, 2004.

[39] C.C. Lin and Y.J. Lee. Stacking sequence optimization of laminated composite structures using genetic algorithm with local improvement. *Composite Structures*, 63:339–345, 2004.

[40] C.C. Lin, Y.J. Lee, and C.S. Hung. Optimization and experiment of composite marine propellers. *Composite Structures*, 89:206–215, 2009.

[41] W. Liu and J. Gong. Adaptive bend-torsional coupling wind turbine blade design imitating the topology structure of natural plant leaves. In Dr. Ibrahim Al-Bahadly, editor, *Wind Turbines*. InTech, 2011.

[42] Z. Liu and Y.L. Young. Utilization of bending-twisting coupling effects for performance enhancement of composite marine propellers. *Journal of Fluids and Structures*, 25:1102–1116, 2009.

[43] D.W. Lobitz and P.S. Veers. Aeroelastic behavior of twist-coupled hawt blades. In *1998 ASME Wind Energy Symposium at 36th AIAA Aerospace Sciences Meeting and Exhibition*, Reno, NV, 1998.

[44] D.W. Lobitz and P.S. Veers. Load mitigation with bending/twist-coupled blades on rotors using modern control strategies. *Wind Energy*, 6:105–117, 2003.

[45] D.W. Lobitz, P.S. Veers, G.R. Eisler, D.J. Laino, P.G. Migliore, and G. Bir. The use of twist-coupled blades to enhance the performance of horizontal axis wind turbines. Technical report, Sandia National Laboratories, 2001.

[46] D.W. Lobitz, P.S. Veers, and P.G. Migliore. Enhanced performance of hawts using adaptive blades. Technical report, Sandia Report 2004, Sandia National Laboratories, 2004.

[47] A. Maheri and A.T. Isikveren. Performance prediction of wind turbines utilizing passive smart blades: approaches and evaluation. *Wind Energy*, 13:255–265, 2009.

[48] A. Maheri, S. Noroozi, and J. Vinney. Combined analytical/FEM-based coupled aero structure simulation of a wind turbine with bend-twist adaptive blades. *Renewable Energy*, 32:916–930, 2007.

[49] I.A. Milne, R.N. Sharman, R.G.J.Flay, and S. Bickerton. A preliminary analysis of the effect of the onset flow structure on tidal turbine blade loads, 2010.

[50] M. Mohan. The advantages of composite material in marine renewable energy structures. In *RINA Marine Renewable Energy Conference*, 2008.

[51] M.R. Motley and R.B. Barber. Passive control of marine hydrokinetic turbine blades. *Composite Structures*, 110:133–139, 2014.

[52] M.R. Motley and R.B. Barber. Passive pitch control of horizontal axis marine hydrokinetic turbine blades. In *33rd International Conference on Ocean, Offshore and Arctic Engineering*, 2014.

[53] M.R. Motley, Z. Liu, and Y.L. Young. Utilizing fluid-structure interactions to improve energy efficiency of composite marine propellers in specially varying wake. *Composite Structures*, 2009.

[54] M.R. Motley and Y.L. Young. Influence of design tolerance on the hydroelastic response of adaptive marine rotors. *Composite Structures*, 94(1):114–120, 2011.

[55] M.R. Motley and Y.L. Young. Performance-based design and analysis of flexible composite propulsors. *Journal of Fluids and Structures*, 27(8):1310–1325, 2011.

[56] M.R. Motley and Y.L. Young. Scaling of the transient hydroelastic response and failure mechanisms of self-adaptive composite marine propellers. *International Journal of Rotating Machinery*, 2012, 2012.

[57] R.F. Nicholls-Lee, S.W. Boyd, and S.R. Turnock. A method for analyzing fluid structure interactions on a horizontal axis tidal turbine, 2011.

[58] R.F. Nicholls-Lee and S.R. Turnock. The use of computational fluid dynamics in the optimisation of marine current turbines. In *10th Numerical Towing Tank Symposium*, Hamburg, Germany, 2007.

[59] R.F. Nicholls-Lee, S.R. Turnock, and S.W. Boyd. Simulation based optimisation of marine current turbine blades. In *7th International Conference on Computer and IT Applications in the Maritime Industries*, Liège, Belgium, 2006.

[60] R.F. Nicholls-Lee, S.R. Turnock, and S.W. Boyd. Performance prediction of a free stream tidal turbine with composite bend-twist coupled blades. In *2nd International Conference on Ocean Energy*, October 2008.

[61] R.F. Nicholls-Lee, S.R. Turnock, and S.W. Boyd. Application of bend-twist coupled blades for horizontal axis tidal turbines. *Renewable Energy*, 50:541–550, 2013.

[62] Northwestern University. Composite materials program. http://www.tam.northwestern.edu/research/composites.html.

[63] A.C. Orifici, I. Herszerg, and R.S. Thomson. Review of methodologies for composite material modelling incorporating failure. *Composite Structures*, 86:194–210, 2008.

[64] B. Polagye and J. Thomson. Tidal energy resource characterization: methodology and field study in admiralty inlet, puget sound, us. *Proceedings of the Institution of Mechanical Engineers, Part A: Journal of Power and Energy*, 227(3):352–367, 2013.

[65] D. Sale, A. Aliseda, and M. Motley. Structural optimization of composite blades for wind and hydrokinetic turbines. In *1st Marine Energy Technology Symposium*, April 2013.

[66] O. Soykasap and D.H. Hodges. Performance enhancement of a composite tilt-rotor using aeroelastic tailoring. *Journal of Aircraft*, 37:850–858, 2000.

[67] Strategic Initiative for Ocean Energy. *Ocean energy: cost of energy and cost reduction opportunities*, 2013.

[68] Strategic Initiative for Ocean Energy. *Ocean energy: state of the art*, 2013.

[69] Strategic Initiative for Ocean Energy. *Ocean energy technology: gaps and barriers*, 2013.

[70] Strategic Initiative for Ocean Energy. *Wave and tidal energy strategic technology agenda*, 2014.

[71] P. Veers, G. Bir, and D. Lobitz. Aeroelastic tailoring in wind-turbine blade applications. In *Windpower '98, American Wind Energy Association Meeting and Exhibition*, Bakersfield, California, 1998.

[72] J. Wang, J. Piechna, and N. Müller. A novel design and preliminary investigation of composite material marine current turbine. *The Archive of Mechanical Engineering*, 58(4), 2011.

[73] B. Whitby and C.E. Ugalde-Loo. Performance of pitch and stall regulated tidal stream turbines. *IEEE Transactions on Sustainable Energy*, 5(1):64–72, January 2014.

[74] A.L. Winter. Differences in fundamental design drivers for wind and tidal turbines. In *OCEANS, 2011 IEEE*, 2011.

[75] R.J.K. Wood, A.S. Bahaj, S.R. Turnock, L. Wang, and M. Evans. Tribological design constraints of marine renewable energy systems. *Philosophical Transactions of the Royal Society A*, 368:4807–4827, 2010.

[76] Y.L. Young. Time-dependent hydroelastic analysis of cavitating propulsors. *Journal of Fluids and Structures*, 23:269–295, 2007.

[77] Y.L. Young. Fluid-structure interaction analysis of flexible composite marine propellers. *Journal of Fluids and Structures*, 24, 2008.

[78] Y.L. Young and S.A. Kinnas. Analysis of supercavitating and surface-piercing propeller flows via BEM. *Computational Mechanics*, 32:269–280, 2003.

[79] Y.L. Young and Z. Liu. *HE PROPCAV User's Manual and Documentation*, 2.0 edition, 2008.

[80] Y.L. Young and Z. Liu. Performance prediction of Newton-Rader propellers. *Journal of Ship Research*, 52(2), 2008.

[81] Y.L. Young, Z. Liu, and M. Motley. Influence of material anisotropy on the hydroelastic behaviors of composite marine propellers. In *ONR NH Symposium on Naval Hydrodynamics*, October 2008.

[82] Y.L. Young, T.J. Michael, M. Seaver, and S.T. Trickey. Numerical and experimental investigations of composite marine propellers. In *26th Symposium on Naval Hydrodynamics*, Rome, Italy, September 2006.

[83] Y.L. Young and M.R. Motley. Influence of material and loading uncertainties on the hydroelastic performance of advanced material propellers. In *Second International Symposium on Marine Propulors*, June 2011.

[84] Y.L. Young, M.R. Motley, and R.W. Yeung. Three-dimensional numerical modeling of the transient fluid-structure interaction response of tidal turbines. *Journal of Offshore Mechanics and Arctic Engineering*, 132, 2010.